LBL-14750

Lawrence Berkeley Laboratory
UNIVERSITY OF CALIFORNIA

Materials & Molecular Research Division

EFFECTS OF WELDING ON WELDMENT MECHANICAL PERFORMANCE IN TWO AUSTENITIC STEELS

Michael Jay Strum
(M.S. thesis)

June 1982

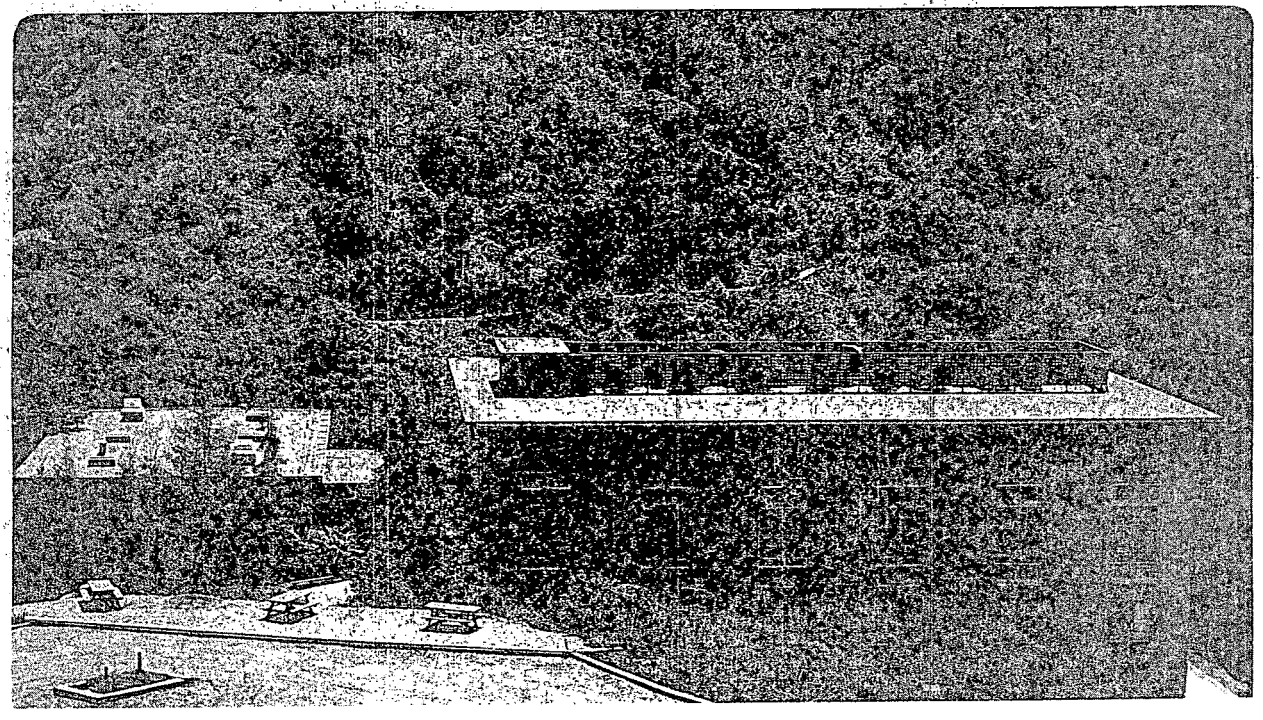

Prepared for the U.S. Department of Energy under Contract DE-AC03-76SF00098

DISCLAIMER

LBL-14750

LBL--14750

DE83 001400

EFFECTS OF WELDING ON WELDMENT MECHANICAL PERFORMANCE IN TWO AUSTENITIC STEELS

Michael Jay Strum

M.S. Thesis

June 1982

MASTER

Materials and Molecular Research Division
Lawrence Berkeley Laboratory
University of California
Berkeley, CA 94720

This work was supported by the Director, Office of Energy Research, Office of Development and Technology, Magnetic Systems Division of the U.S. Department of Energy under Contract DE-AC03-76SF00098.

Table of Contents

Effects of Welding
on Weldment Mechanical Performance in Two Austenitic Steels

Master of Science | Michael Jay Strum | Materials Science and Mineral Engineering

J.W. Morris, Jr.
Chairman of Committee

ABSTRACT

The effect of autogenous gas-tungsten arc-welding on the mechanical performance of two austenitic steels has been evaluated. The materials were candidates for use as the jacket material in a force-cooled superconducting magnet cable operating at 4K with critical stress levels of up to 1035 MPa (150 ksi). The original candidate material was Nitronic 40, a nitrogen-strengthened stainless steel. Although strength levels were promising, an in-situ reaction heat treatment at 700°C necessary for the formation of the superconducting A15 phase results in severe degration of the tensile ductility in the weld metal at cryogenic temperatures. Transformation of the residual delta ferrite present at dendrite cores in the weld metal solidification structure provides a brittle network of products believed to be sigma phase. Base metal toughness also deteriorates, with the precipitation of carbo-nitrides at 700°C leading to intergranular fracture at cryogenic temperatures. The search for an alternate material led to JBK-75, a modified A-286 type γ' precipitation hardening iron-based superalloy. Welded in the solution-annealed condition, the subsequent reaction heat treatment provides a conventional aging treatment for the entire weldment. This material was eventually selected for use by the manufacturers

of the magnet coil.

However, observations of a tensile strength mismatch between base metal and the weaker weld metal in JBK-75 prompted a further study into the aging response in weldments of this alloy. Electrical resistivity measurements during isothermal aging indicate a significant difference in the precipitation kinetics of base and weld metals, with a faster initial response in weld metal samples. But hardness aging curves display a persistent mismatch between base and weld hardness levels with weaker weld metal regions displaying a slower aging response. This disparity is explained with the documentation of titanium segregation to the interdendritic regions of the weld solidification structure. Although titanium enriched regions may show rapid initial precipitation, resultant weld metal strength increases are abated by regions of titanium depletion. Observations of localized strain through slip step traces confirm the presence of an easy-path of deformation within the solidification structure. Weldment strength is also seen to vary with grain size as evidenced by microhardness taverses through the weld zones. Finally, it was found that through post-weld annealing treatments at 950°C, prior to aging, weldment hardness levels can be matched. However, although increased strength levels are obtained in the weld metal, concomitant decreases in base metal strengths are suffered, presumably due to observed grain growth.

1.0 INTRODUCTION

The most effective method for joining metals is often by a welding process. In the simplest case this involves the application of intense heat to form a molten pool bridging two butted plates, and the resolidification of this weld metal. The weldment resulting from this joining process is no longer a homogeneous structure and cannot be fully characterized by base metal properties alone. It is now a composite of weld metal and weld heat affected zones (HAZ), in addition to base material.

This work examines the effect of gas tungsten arc (GTA) autogenous butt welding two austenitic steels on their mechanical performance. A nitrogen strengthened austenitic stainless steel, Nitronic 40, displays increased susceptibility to brittle fracture in the weld after a 700°C heat treatment. And JBK-75, a modified A-286 type iron-based supperalloy displays a significant variation in aging response and resultant mechanical properties between base and weld metal regions.

Study of these materials was initiated in response to the needs of the Fusion Energy Program for evaluation and selection of a cable jacket material for use in a force-cooled superconductor coil design. Use of an unconventional superconducting wire, Nb_3Sn, in this coil is warranted by its superior critical-field and critical-temperature values (1,2). Because the superconducting A15 phase in Nb_3Sn is extremely brittle, a bronze-process technique is used. The conductor is initially composed of fine multifilaments of niobium and bronze. These are bundled into a cable and encased in a protective metal sheath or jacket 1.7 mm in thickness. This jacket is then gas-tungsten-arc (GTA) seam welded along its entire length. After compaction to 32% void fraction the conductor is

wound into the final coil configuration. A reaction heat treatment of 700°C for 30 hours causes formation of the superconducting A15 phase, Nb_3Sn, by a solid state diffusion reaction. Forced flow of supercritical liquid helium through the interstices of the multifilamentary cable confined by the surrounding jacket is used to keep the windings cooled below their critical temperature.

During normal operation the conductor sheath is expected to experience pressure-induced stresses of 200-275 MPa. However, during fault conditions the local stresses, due to boiling liquid helium coolant may approach 1035 MPa (3). The proposed jacket material acceptance criteria listed in Table 1 include superior strength, good toughness and accommodating ductility. Low magnetic permeability and metallurgical stability at 4.2K are additional requirements.

The originally proposed candidate jacket material was Nitronic 40, an austenitic stainless steel strengthened with interstitial nitrogen. Strength levels in the alloy were very promising. But this investigation demonstrates an incompatability of the weldment with the reaction heat treatment, nominally 700°C for 30 hours.

Typical of austenitic stainless steels, the chemistry of this alloy is adjusted to form a small amount retained primary delta-ferrite on solidification to prevent microfissuring (4-6). It is proposed that this metastable delta-ferrite retained at the dendrite cores after welding decomposes into sigma phase during the heat treatment. This results in very poor tensile ductility at cryogenic temperatures due to an almost continuous fracture path of brittle sigma phase.

Modifications of alloy chemistry to prevent retention of delta-ferrite after welding were not attempted, although mircofissuring is not

generally a problem in single-pass welds or thin plate (4,7). Base metal toughness is also seen to deteriorate with precipitation of grain boundary carbonitrides occurring during the reaction heat treatment at 700°C.

The search for an alternate material led to preliminary evaluations of JBK-75. JBK-75 is an iron-based superalloy precipitation hardened by a fine dispersion of gamma-prime in the autensite matrix. The alloy is similar to A-286, but modified to increase high temperature strength and ductility leading to improved hot cracking resistance (8,9). This involved removal of Mn and Si additions and lowering B and C levels while increasing the amount of Ni. Welded in the solutionized condition, the reaction heat treatment for the superconductor provides a conventional age hardening treatment for the entire jacket weldment. Testing at 4K at the Westinghouse Research and Development Laboratory (3) using a different heat of JBK-75 in the fully processed condition resulted in strength levels surpassing the proposed acceptance criteria. The simulated fully processed testing condition includes an assumed uniform 10% cold work the weldment receives during compaction of the conductor before the reaction anneal of 700°C for 30 hours. On the basis of these and other tests, JBK-75 was chosen for use as the conductor jacket material in the Westinghouse-Airco Large Coil Project (LCP) magnet coil.

The bulk of this work investigates the effect of gas-tungsten-arc (GTA) autogenous butt welding on the aging response and structure-property relationships in JBK-75. This was prompted by tensile test observations of a persistent strength mismatch between base metal and weaker weld regions. Knowledge of the base metal aging response alone is therefore no longer sufficient to optimize weldment mechanical performance.

This strength mismatch can have large consequences in applications where the weld metal is subjected to stress similar to those in the rest of the weldment. The stress levels applied to the structure are now limited by the fracture strength of the weaker weld. Additionally, although the weld may be very ductile, accommodational strains will be concentrated in the weaker weld region resulting in failure after relatively small total strains. Total strain before failure will continually decrease with increasing effective gage lengths which include the weld region. Of course, the magnitude of these problems will depend on the degree of strength mismatch present.

In an attempt to discover the origin of the strength mismatch, weld metal and base metal aging responses are studied. Differences in aging response are very important to the strength levels attained in this primarily precipitation-hardened alloy. Resistivity measurements during isothermal aging at 725°C are used to obtain information on early stage precipitation. Hardness curves of base metal and weld metal regions are used to determine the effect of aging time and treatment on strength. Hardness curves of weldments both with and without 25% post-weld cold work before aging at 725°C are examined.

Two major factors seem to influence the decreased hardness level in the weld. The first is the dendritic solidification structure. Segregation of titanium, the major hardening element in JBK-75, to the dendrite interstices is verified using Auger Electron Spectroscopy. The effect of titanium segregation on the weld metal aging response is examined by hardness measurements and deformation induced slip-step observations. These tests were performed both before and after post-weld annealing treatments at 950°C. The effect of these post-weld treatments on homogeni-

zation of the weld is evidenced by the reduction in localized deformation within the weld solidification structure.

The second factor contributing to the mismatch is the larger columnar grains in the weld metal relative to the fine equiaxed base metal microstructure. Microhardness traverses across the weld zones display the effect of increased grain size in both the weld and heat affected zones. Recrystallized weld metal grains, achieved through a post-weld thermomechanical treatment, further indicate the magnitude of the grain size effect on the mismatch by matching base metal and weld metal grain sizes for hardness comparison. Significant reductions in the as-solidified weld metal grain size is difficult in a fully austenitic steel, and beyond the scope of this work. However, some success has been achieved by others using mechanical vibrations, arc or torch modulation, magnetic stirring, and carbide impregnation (10-13).

2.0 EXPERIMENTAL PROCEDURE

2.1 Material Histories

A. Nitronic 40

Nitronic 40 is a nitrogen strengthened stainless steel, nominally in wt.%, 21 Cr, 6 Ni, 9 Mn. The materials used in this investigation were from commericial heats produced by the Armco Steel Corporation. Tensile specimens were machined from 1.5 mm thick sheet. Charpy specimens were machined from 10.7 mm thick plate. Both sheet and plate were fully homogenized and annealed as received. Chemical analyses are listed in Table 2.

Base metal test specimens were either as-annealed at 1000°C, cold rolled to a 10% reduction, or cold rolled and aged 20 hours at 700°C. Welded test specimens from annealed sheet were either as-welded or welded and aged 30 hours at 700°C. All specimens were sealed in stainless steel bags prior to any furnace heat treatment.

B. JBK-75

JBK-75 is a modified A-286 type iron based superalloy with improved weldability. Two heats of material were used in this investigation. The first heat was used for preliminary candidate material testing including all tensile tests. The second heat of material was used for the subsequent study of weldment aging response. Both heat chemistries are listed in Table 3 along with the nominal composition of standard A-286 for comparison purposes.

The first heat of material was received as a 25 mm by 75 mm block 250 mm long. It was homogenized 24 hours at 1200°C and air cooled then

hot rolled at 1000°C from 25 mm to 6.3 mm thickness. All visible surface scale was machined off. The material was then cold rolled to a 1.5 mm thickness, solution annealed 1 hour at 950°C and water quenched in its sealed stainless steel protective bag.

The second heat is part of an especially homogenious ingot used by Headley et al (14) in a separate study of the precipitation sequence in this alloy. The material was received as 50 mm diameter rod, vacuum induction melted and vacuum arc remelted, homogenized 72 hours at 1190°C, and extruded at 990°C. It was subsequently hot rolled at 1000°C to 13 mm thick plate and water quenched, descaled using a 120 grit belt grinder and cold rolled to 3.2 mm thick sheet. Solution annealing for 1 hour at 900°C was followed by a water quench of the sealed stainless steel bag. Solution anneal treatments for both heats of material resulted in greater than 95% recrystallization. The resultant grain sizes were both between ASTM 9 and 10.

All welding was performed on sheet in the as-solution annealed condition. Aging treatments were carried out at both 725°C, 700°C and double aging treatments at 650°C all followed by air cooling. Pre-age cold work for a hardness curve study was achieved by cold rolling the entire weldment after first grinding the surfaces flush.

2.2 Welding

All welds in this study were autogenous (without filler metal) gas-tungsten arc welds (GTAW). The exclusive joint configuration consisted of two plates with squared edges butted together. Plate sizes ranged from 1.5 mm to 3.2 mm in thickness. As mentioned previously, all welding was performed on material in the solution annealed condition.

Weld preparation began with cutting the plates using a horizontal band saw to create parallel and square joint surfaces. The material was then cleaned using a 120 grit grinding belt until all visible scale was removed. Just prior to welding, the plates were degreased with acetone.

The weld set-up consisted of the two butted plates clamped to a copper block with machined grooves and several small holes allowing inert gas to flood the underside of the weld joint. The Nitronic 40 and the earliest JBK-75 welds were performed by professional welding technicians. Later welds were automated using a motorized carriage system to translate the torch along the joint seam. The power supply used is a Miller Syncrowave 300.

Full penetration welds were achieved in every case. Welding conditions adopted were DC straight polarity with 2.4 mm diameter thoriated tungsten electrodes using a 40° included angle and argon as both the shielding and backing gas. Typical weld heat input variables as monitored for both 1.5 mm and 3.2 mm thick welds are listed in Table 4.

2.3 Resistance Measurements

Electrical resistance levels were monitored during the isothermal aging of base metal or weld metal strip samples. Using a constant current power source any resistance changes resulted in a change of potential across the sample. Using current levels of approximately one ampere the potential drops across 50 mm of the 75 mm long samples were about 30 millivolts. Using a voltage offset (suppression) device, the sensitivity of the Gould model 110 recorder was set to one millivolt full scale deflection. Both current and voltage leads of high temperature Kanthal A-1 Fe-Cr-Al-Co furnace element wire were spot welded onto the strip

samples. A thermocouple was attached to the center of the sample for temperature records. The aging treatments were performed at 725°C in a 25 mm diameter, 0.6 m long tube furnace in argon. The experimental set-up is shown in Figures 1 and 2.

Before insertion of the samples, the electronics were allowed to stabilize a minimum of one hour. The relatively large temperature dependence of the resistivity required adjustment of the voltage offset near the terminal temperature. Therefore the initial resistivity (voltage) was chosen as that after one minute at temperature. The data plotted are the percentage change in this initial resistivity as a function of aging time. Two tests of each the base metal and weld metal samples were performed. The data presented are the average of the two experimental curves obtained for each sample type.

2.4 Mechanical Testing

A. Hardness Tests

Hardness testing was performed on both base metal and weld metal regions. After welding and heat treating, the specimens were ground until both top and bottom surfaces were flat and parallel using a surface grinder with an aluminum oxide wheel. Specimens were then polished through a series of SiC wet papers of grit sizes 240 to 600. Resulting specimen thicknesses were approximately 2 mm. Lastly, the specimens were macro-etched in Keller's concentrated etch of mixed acid in distilled water. This allowed centering of the indentor during hardness tests on the weld centerline, improving the accuracy and consistency of weld metal hardness data.

A Wilson Rockwell hardness tester was used for the hardness measure-

ments. For samples harder than R_c 20, 'C' scale tests were used with a 150 kg major load and diamond brale indentor. An escape time of 20 seconds was set as standard. Softer samples were tested on the 'B' scale with a 100 kg major load and a 1.6 mm steel ball indentor. Using a Wilson conversion chart these values were converted into equivalent 'A' scale values for data presentation. At least six indentions were made and the readings averaged for each data point. The error bars in the hardness curves are average values plus or minus the standard deviation in the readings.

B. Microhardness Tests

Microhardness measurements were made on a Leitz Miniload 2 microhardness tester using a diamond pyramid indentor. Metallographic specimens were prepared from weldments in an identical manner to that used for optical metallography. Indention diameters were measured to the nearest tenth of a micrometer in both directions, averaged and converted into Vickers Hardness values. A load of 1000 gm was used with a 15 second plunge time and 25 second test time taken as standard. Hardness traverses across the weld zones were repeated three times. The average values obtained from each set of three tests corresponding to equivalent regions in the weldment are plotted in the presented figure.

C. Tensile Tests

Tensile tests were performed using ASTM standard flat tensile specimens with 25.4 mm gage lengths. Weldment specimens were cut such that the weld metal region was centered on the gage length with the tensile direction transverse to the weld length and ground flat. There-

fore weld metal, HAZ and base metal regions were all included in the gage lengths of the welded test specimens. Gage marks were scratched onto the specimens and measured both before and after testing using a travelling microscope with an accuracy of $\pm$0.01 mm. Gage lengths of 6.35 mm, 12.7 mm and 25.4 mm were used on welded specimens to indicate the relative ductility of the weld metal in the composite specimen. Total elongations were thus measured directly. Reduction in the area data were extrapolated from measurements of maximum reductions in gage widths. The yield strengths reported were found using 0.2% offset strain levels. Strain rates were either 0.5 or 1.0 mm/min. Cryogenic testing at 77K and 4.2K was accomplished by complete immersion of the tensile specimen in liquid nitrogen or liquid helium during testing using a compression tube and appropriate cryostat.

D. Localized Deformation

Localized deformation was studied through observations of deformation induced slip steps on specimen surfaces. Weldment specimens were ground flat and parallel with a surface grinder and both rough and fine polished on both sides to produce a metallographic quality finish. The specimens were then loaded in compression transverse to the weld length to induce dislocation motion. The as-polished and deformed specimens were observed in an optical microscope using polarized light.

2.5 Microscopy

A. Optical Metallography

Optical metallography was conducted on a Carl Zeiss Universal Photomicroscope Ultraphoto II. Most samples were mounted in thermo-

setting plastic. Rough grinding on a 180 grit belt was followed by wet grinding through a series of four papers 240 grit to 600 grit. Fine polishing was carried out on rotating platters covered with cloths impregnated with 6 μm, then 1 μm diamond paste. Most samples were etched in Keller's concentrated etching solution (10% HF, 25% HNO_3, 15% HCl, in distilled water).

B. Scanning Electron Microscopy

Tensile specimen fractography and phase identifications by chemical analyses were all performed in a scanning electron microscope (SEM) with a Kevex X-ray detector and analyzer. The microscope used was an AMR 1000 operated at 20 kV. The SEM was also used for improved resolution of microstructural detail in metallographically prepared, polished and etched specimens at high magnifications.

C. Scanning Auger Spectroscopy

Scanning Auger Spectroscopy allows surface chemical analysis for all elements of atomic wt. greater than B. This technique was used for documentation of segregation in as-solidified weld metal through the generation of concentration profiles across the solidification substructure. These line profiles were produced using a 1 μm beam size to scan approximately 100 μm of weld. The peak to peak amplitude of the differentiated intensity signal (dN/dE) of the desired element (Ti) was plotted versus position. The curve was calibrated to atomic percent titanium using spot composition analyses of the alloys' four major elements at five known locations along the line scan. The microscope used was a Physical Electronics Model Phi 590 'Super-Sam'.

3.0 RESULTS AND DISCUSSION

3.1 Material Selection and Evaluations

A. Nitronic 40

The initial selection for use as the conductor jacket material was Nitronic 40. This is a Cr-Ni-Mn austenitic stainless steel solid solution strengthened with nitrogen. Although both weldability and 4.2K tensile strength and ductility in this alloy are excellent, this investigation sought to identify its degree of compatability with the reaction heat treatment of 700°C for 30 hours. It is well known that many austenitic stainless steels are susceptible to weld decay phenomena and sensitization reactions when subject to temperatures between 450°C and 900°C (15-17). However, the problem most usually encountered is with localized corrosion. Precipitation of grain boundary chromium-carbides in weld heat affected zones or base metal leave adjacent areas depleted in chromium and very susceptible to corrosive effects. Although the conductor jacket will not operate in a corrosive environment, it is shown that the reaction heat treatment is detrimental to cryogenic temperature mechanical performance. Tensile ductility in welded specimens is severely reduced at 77K, and base metal Charpy Impact Energy values also drop after the heat treatment, especially at 77K. Both of these mechanical property phenomena are correlated with microstructural changes occurring during heat treatment at 700°C and result in observable variation in the fracture morphology.

Tensile tests of Nitronic 40 were performed on base metal both as cold worked 10% after solution annealing 2 hours at 1000°C, and cold worked 10% before aging at 700°C for 30 hours. GTA welded tensile specimens tested were either as welded or welded and aged 30 hours at

700°C. The results of the tensile tests are given in Table 5. Base metal tensile properties were acceptable in every case giving no obvious indication of embrittlement after aging. Specimens tested at 4.2K after 10% cold work and aging resulted in an impressive yield strength of 212 ksi and 16% elongation. However, GTA welded and aged specimens displayed extremely poor tensile ductility at 77K. The aging treatment appears to cause a ductile to brittle transition between 298K and 77K. Elongations at 77K dropped from 13% in the as-welded condition to only 1% after aging.

The as-welded microstructure, as shown in Figure 3 is composed of primary delta ferrite in an austenitic matrix. The delta ferrite displays a vermicular morphology at the cores of the originally solidified dendrites. The aged weld in Figure 3, however, displays distinctive contract after a similar electrolytic etch in oxalic acid. It has been reported elsewhere that with electrolytic etching techniques, delta-ferrite remains in relief while carbides and sigma phase are attacked (18). Comparison of the tensile fracture surfaces with the polished and etched weld microstructures in Figure 4 are also quite revealing. In the as-welded tensile specimen tested at 77K there is no obvious relationship between the microstructure and the ductile fracture mode. However, at 77K after aging, the fracture directly follows the boundaries of the second phase constituent observed in the microstructure. This provides an almost continuous fracture path.

It is proposed that the aging treatment of 700°C for 30 hours has caused the delta ferrite to decompose into the tetragonal sigma phase. Singhal and Martin (19) have shown that sigma phase tends to nucleate on ferrite-austenite boundaries. Ferrite is then preferentially consumed

during the growth of sigma. It has been shown by Savage and others (20-22) that the retained primary delta ferrite in stainless steel welds is enriched in chromium and depleted in nickel. Growth of the tetragonal (Fe_4Cr) sigma phase should be encouraged by these conditions.

The amount of delta ferrite present in a weld is usually determined by calibrated magnetic permeability measurements (23-26). Permeability measurements of Nitronic 40 welds (see Table 6) using a Severn gage indicate the reduction of the magnetic delta-ferrite phase to below detectable levels after aging. This is expected since delta ferrite is not a stable phase in Nitronic 40 and is not present in the base metal.

The embrittling solid-state transformation of the delta ferrite could be avoided by manipulation of the weld chemistry by nitrogen additions to the shielding gas for example, resulting in ferrite-free welds. But these and other possible attempts to increase weld metal ductility after aging were dismissed due to indications of base metal sensitization. Charpy impact energy test data (27) indicates brittle base metal behavior at 77K after 10% cold work and aging (see Table 7). Fractographic observations (see Figure 5) clearly reveal an increasing tendency toward intergranular fracture in the aged specimens. This correlates well with microstructural observations of semi-continuous carbo-nitride precipitates at the grain boundaries after aging. These precipitates were identified (27) by the presence of carbon and nitrogen peaks in precipitate surface analysis using scanning auger spectroscopy. With both base metal and weld metal properties deteriorated below acceptable limits by the reaction heat treatment, search for a replacement alloy began.

B. JBK-75

The search for an alternate conductor jacket material led to the iron-based superalloys. A modified A-286 type alloy, JBK-75 was chosen for evaluation due to its improved resistance to hot cracking. The reaction heat treatment for the superconductor could now be used to strengthen the precipitation hardening jacket material. This allowed welding in the solution annealed condition, resulting in maximum uniformity of mechanical properties through the weld zones on aging.

But early tensile tests of weldment specimens at 298K and 77K displayed both low yield strengths and a modest temperature dependence of the yield strength. Later testing of similar specimens at a facility capable of liquid helium temperature tensile tests, exhibited a much improved yield strength at 4.2K after the reaction heat treatment of 30 hours at 700°C, (see Table 8).

Meanwhile hardness curves at 700°C, 725°C and 750°C were produced to indicate the relative strength level after the nominal aging treatment. These curves indicated that the nominal treatment left the material underaged. Peak hardness in the base metal appeared to require 50 hours at 725°C. The hardness curves are not reproduced here due to a large amount of data scatter and were used for indication only. These problems stemmed from the 1.5 mm thin starting material. Bead-on-plate welds were too narrow for consistent sampling by the Rockwell indentions. And it appears that after belt grinding the weldment specimens flat, the samples were thin enough that fluctuations in sample thickness caused the scatter in base metal hardness levels. The base metal curves did indicate typical precipitation hardening behavior. Peak hardness was reached

faster at higher aging temperatures but the corresponding peak hardness values decreased. This is the basis for the double aging treatments performed at 725°C and 650°C. Increased hardness can be obtained consistent with relatively short aging times by aging to near the peak hardness at the higher temperature followed by aging at the lower temperature.

Using the aging treatments suggested by the hardness results in an effort to discover the alloy's strength potential, tensile specimens were prepared. Tensile test results, shown in Table 9, display much improved yield strengths at 77K. The specimens given 10% cold work prior to aging display an additional significant strength increase, suggesting a related improvement in the aging kinetics.

However, a persistent strength mismatch exists between base metal and weldment specimens. Although all fracture surfaces indicate ductile rupture, weldment specimens consistently failed in the lower strength weld metal. This resulted in low total elongations over the 25.4 mm gage even though the weld metal was very ductile as evidenced by the reduced gage length elongation data. The lower strength weld metal thus causes strain localization in the weldment specimen. The magnitude of this strength mismatch was observed to decrease with test temperature as shown in Figure 6 and Table 10. This may be rationalized by an increased resistance to the slip localization within the weld solidification structure, discussed later, due to increased resistance to the cross-slip of screw dislocations at cryogenic temperatures.

A separate evaluation of JBK-75 in the fully processed condition was conducted at the Westinghouse Research and Development Center (3). With 10% cold work prior to the nominal reaction heat treatment of 30 hours at 700°C, all of the original acceptance criteria were exceeded. JBK-75 was

therefore chosen for use as the conductor jacket material in the Westinghouse-Airco Large Coil Project superconducting coil. Differences in tensile data are not fully understood at this time but may stem from variations in heat chemistries, ingot homogenization and welding conditions.

3.2 Weldment Aging Response

The persistent strength mismatch observed between weld metal and base metal regions prompted the investigation of weldment aging response in the iron-based superalloy JBK-75. Early stage precipitation information is obtained from resistance measurements during isothermal aging. Hardness curves provide resultant strength level indications as the precipitation sequence progresses. Microstructural correlations of weldment mechanical anisotropy focus on the differences between the as-cast weld metal and the homogenized equiaxed base metal microstructures. Chemical inhomogeneity in the weld is documented with line scans of the titanium concentration profile across the dendritic and interdendritic regions of the solidification structure. Grain size effects in the weldment are observed in microhardness traces across the weld zones, and observation of slip step traces in deformed weldments define regions of high local strain.

A. Resistance Curves

The resistance curves, shown in Figure 7, are plots of electrical resistivity changes occurring during isothermal aging at 725°C. The resistance increases are mainly due to the formation of Guinier-Preston zones, the earliest stage of precipitation. It is believed (28-30) that

the resistivity maximum is associated with a critical zone diameter of about 10Å causing maximum scattering of the conduction electrons. The maximum resistance increase should then be proportional to the density of zones of approximately critical diameter. Both smaller and larger size zone diameters should result in decreased resistivities.

Comparison of the base metal and weld metal resistance curves evidence a faster aging response in the weld metal. The time to peak resistance is only about twenty minutes in the weld metal versus fifty minutes in the base metal samples. But the weld metal samples also exhibit a lower peak resistance increase and a more rapid decrease relative to base metal samples. Although the resistance method is very sensitive to early stage precipitation no evidence of latter stage equilibrium precipitation was seen. Interpretation of observed differences between the two curves will be discussed later using weld metal segregation arguments.

B. Hardness Curves

Hardness-aging curves provide resultant strength level indications as the precipitation sequence progresses during isothermal aging. Both base metal and weld centerline hardness curves are each plotted in Figures 8, 9 and 10. These display the weldment aging responses at 725°C and 700°C in the as-welded condition and at 725°C after 25% post-weld cold reduction respectively. In each case the weld metal exhibits a slower age-hardening response, lower peak hardness and persistent strength mismatch with the base metal. It can also be seen that the weld metal continues to harden long after the base metal has reached its peak level and begun to soften or overage.

Although the weld metal hardness approaches that of the base metal

after very long aging times at 725°C, this is not a practical heat treatment. Both base metal and weld metal possess significant amounts of a cellular grain boundary phase believed to be the equilibrium eta phase, Ni_3Ti, after 125 hours at 725°C. This phase heterogeneously nucleates and grows from the columnar grain boundaries in the weld, as seen in Figure 11. The large misfit between the HCP equilibrium eta phase and the FCC matrix favors precipitation of the metastable ordered FCC gamma-prime precipitates at low aging temperatures and short aging times (31-33). However, no indication of the precipitation of the cellular phase appears on the hardness curves. Thus it appears that the hardness behavior after long aging times is governed more by the overgrowth of gamma-prime precipitates to sizes allowing dislocation by-passing than by the presence of the cellular phase. However, presence of the cellular phase, forming brittle grain boundary layers must usually be avoided.

From early tensile results of weldments given 10% cold work prior to aging it appeared that such treatments may be beneficial in reducing weldment anisotropy. But even after 25% uniform cold work prior to aging the large mismatch persists. However, the aging response is greatly accelerated, with peak base metal hardness occurring after only one hour. Weld hardness continues to increase as base metal softens but reaches a plateau after only four hours at 725°C. The peak hardness levels are much improved with the weld hardness peak approaching the base hardness peak level in the as-welded and aged condition.

C. Segregation

Segregation during weld solidification is usually identified with hot cracking problems. Typically, solute rejection at the advancing

solid/liquid interface results in the formation of low melting-point eutectics or solute-rich regions at the dendrite interstices (8,34-37). Shrinkage strains cause the initiation and propagation of cracks through these low strength regions still near their melting points. A-286 is an alloy well known for its high susceptibility to weld hot cracking when welded under conditions of high restraint as in thick sections. This susceptibility was drastically reduced in JBK-75 by modification of the equilibrium and properties of the segregated low melting phase through removal of Si and Mn additions and lowering B and C while increasing Ni levels (8,9). However, although cracking problems were not encountered in this investigation, segregation of titanium, the major hardening element, to interdendritic regions on solidification is shown to alter the subsequent aging response and strength levels in the weld.

The presence of segregation in JBK-75 welds is evidenced by severe coring upon etching. This allows observation of the solidification structure in Figures 12 and 13 due to the preferential attack of dendritic regions with a mixed-acid etching solution. Solute rejection of titanium to the interdendritic regions is evidenced by the presence of small titanium-rich precipitates exclusively at the dendrite interstices in as-welded specimens. These precipitates include both the titanium and titanium-molybdenum carbides found randomly dispersed in the base metal and a highly substituted phase believed to be the $(Fe,Ni,Cr)_{24}(Ti,Mo)_5$ topologically close-packed χ phase often found in A-286 (32,38,39) but not reported in a thorough study of JBK-75 base metal precipitation (14). These precipitates were identified from Kevex quantitative chemical analysis in the scanning electron microscope.

The magnitude of titanium segregation has been documented by Auger electron spectroscopy. Line scans across the solidification structure give the concentration profile of titanium in Figure 14. The nominal 2.5 At% titanium concentration is seen to fluctuate between a minimum of 1.0 At% at dendrite cores to maxima of about 5 At% at interdendritic regions, with a 1 μm beam size. Spot analyses along the line scan revealed no indication of Ni, Cr, or Fe segregation.

These large variations in titanium concentration within the solidification structure result in a non-uniform aging response in the weld metal. The titanium enriched regions are expected to display both rapid initial precipitation of γ' and a higher density of nucleii due to increased supersaturation. Titanium depleted regions are expected to possess fewer nucleii with corresponding large average precipitate sizes. These phenomena were observed by Clark and Pickering (40) using transmission electron microscopy in 15Cr, 25Ni, iron-based alloys with titanium contents between 2.0 and 3.85 wt.%. Similarly Owzcarski and Sullivan (41) have reported observations of large γ' particles formed near the solvus temperature in a welded nickel-based superalloy which delineate the regions of coring of the original as-cast structure. The resistance curve data can thus be interpreted as consistent with the expected aging response. The rapid initial resistance increase in the weld metal specimen can be associated with rapid precipitation in titanium enriched regions. The lower peak resistance increase and more rapid decrease are consistent with early coarsening above the 10Å critical precipitate diameter of both the titanium enriched regions and the titanium depleted regions.

The segregation of titanium resulting in non-uniform precipitation behavior also affects the hardness levels in the weld metal. In an aging study of a series of Fe-15% Cr-20% Ni-Ti steels with titanium contents of 1.5 to 3.75% by Blower and Mayer (42), hardness levels were seen to increase steadily with increasing titanium content after any identical aging treatment up to 100 hours at either 700°C or 750°C. It was also observed that to obtain useful hardening, the free titanium content must be greater than 1.5%. The weld metal should therefore consist of locally hard and soft regions, corresponding to the local concentration of titanium. Although the solidification structure is too fine to isolate dendritic or interdendritic regions for microhardness testing, preferential deformation between these regions has been observed.

D. Localized Deformation

Localized deformation in the weldment and within the weld solidification structure is observed by the presence of slip steps. As-polished weldment samples plastically deformed in compression leave slip step traces on the specimen surfaces observable under polarized light in the optical microscope. The welded and aged specimen shown in Figure 15 exhibits two levels of localized deformation. First, the weld metal has been strained much more than the HAZ region on the right-hand side of the figure. This follows from tensile and hardness level data showing a significant strength mismatch between base metal and weaker weld metal regions. Secondly, there is an observable localization of strain within the weld solidification structure itself. This localized strain is the result of an 'easy-path' of deformation following the dendritic regions within the weld. Preferential deformation of these low titanium concen-

tration regions leave surface topography delineating the cored regions of the solidification structure.

The hardness decrease in the weld metal due to an 'easy-path' of deformation should be proportional to the degree of titanium depletion at dendrite cores. Therefore weldments were given post-weld solution anneal treatments to reduce the severity of segregation in the weld metal. An as-polished and deformed weldment specimen given a post-weld heat treatment of 10 hours at 950°C before aging is shown in Figure 16. With the exception of a few traces of primary arm dendrite cores, the localized deformation within the solidification structure has disappeared. It can also be seen that localized strain of the weld metal region has been replaced by much more uniform strain throughout the weldment. This displays the achievement of a close match of strengths in the weldment unobtainable through conventional aging treatments. This is further illustrated by the hardness curves in Figure 17. The post-weld anneals are seen to greatly increase the hardness levels in the weld metal after aging. Weld metal hardness values increase from R_c 22 when aged 24 hours at 725°C after welding to above R_c 30 when given the same aging treatment after a solution anneal of 10 hours at 950°C. This appears to be due to more uniform distributions of titanium resulting in more homogeneous precipitation within the weld metal. Therefore previous easy-paths of deformation are reduced or effectively removed.

Hardness levels in as-annealed weld specimens are given in Figure 18. The continued low hardness levels prior to aging display the dependence of the hardness increases on improved weld metal aging responses. Although these as-annealed specimens were observed to contain cellular products in the weld at dendrite interstices in excess of that observed in the

as-welded microstructure, the associated decreases in hardness levels upon annealing indicate only a possible detrimental effect by their presence. For toughness considerations it would most likely be desirable to perform the post-weld annealing treatments above the solvus temperature of the cellular products. Observed hardness decreases in the base metal upon annealing correlate well with observed grain growth, but weld metal grain growth was not apparent.

Although the annealing treatments do not come close to fully homogenizing the weld, a significant reduction in coring is observed in the polished and etched microstructure. The solidification structure of the annealed weldment in Figure 19 is very faint relative to the as-welded sample as viewed under identical conditions in the optical microscope. This may be due in part to the removal of low angle boundaries between dendritic and interdendritic regions during annealing. However, clear observations of localized deformation in a recrystallized weld specimen (see Figure 20), proved these low angle boundaries have little effect on the observance of as-deformed contrast. Localized deformation between dendritic and interdendritic is evident even though recrystallization has occurred. From the large hardness increase in the weld metal after only one hour at 950°C, small increases in titanium concentration must cause significant increases in the level of titanium supersaturation at the dendrite cores. This seems reasonable since Blower and Mayer (42) found that titanium concentrations greater than 1.5% were required to obtain useful precipitation behavior in similar alloys. Thus rapid increases in titanium supersaturation at aging temperatures are expected in regions of near 1.5% titanium concentration upon annealing.

E. Grain Size

Another factor limiting the weld metal strength is the large columnar grains formed on solidification. These grains are composed of packets of similarly oriented dendrites, as can be seen in Figure 21. The large disparity between weld metal and base metal grain sizes is readily apparent. This figure shows the indentions made during weldment microhardness traverses. The results, plotted in Figure 22, display the significance of grain size on hardness. The finer grained weld metal near the fusion boundaries exhibit increased hardness levels and the enlarged heat affected zone base metal grains exhibit decreases in hardness. The decrease in base metal hardness after annealing treatments is explained by this grain growth.

In order to expose the magnitude of the strength mismatch dependent on grain size differences, the entire weldment was recrystallized. After 25% uniform cold work the weldment was recrystallized/annealed one hour at 950°C. This produced equiaxed weld metal grains matching the grain size of the base metal at ASTM #6. As can be seen in Figure 23 the resultant grain size is much finer than the original columnar grains still visible through observation of the as-cast dendrite orientations in the polished and etched microstructure. Although the presence of segregation is evident from the cored microstructure, significant hardness increases are expected due to the annealing treatment alone. Figure 24 compares the base metal and weld metal hardness levels upon aging of as-welded, annealed and recrystallized weldment specimens. The graph shows that the matched base and weld metal grain sizes still result in a weaker weld even though weld hardness levels were improved. As-recrystallized (unaged) specimens on the other hand possess matching microhardness levels, with the weld slightly harder at 156 HV versus base metal at 152 HV. These

results further emphasize the importance of the aging response in determining final strengths in this alloy.

4.0 CONCLUSIONS

A. Nitronic 40 Weldments

Nitronic 40 autogenous weldments exhibit very poor tensile ductility at 77K after exposure at 700°C.

A brittle fracture path is provided by the transformation products present at dendrite cores from the consumption of the delta ferrite remaining after weld metal solidification.

B. JBK-75 Weldments

1. A persistent strength mismatch exists in autogenous JBK-75 weldments between base metal and weld metal regions. This can be attributed to both:

   a) Microstructural coarseness from the large columnar weld metal grains.

   b) Chemical segregation of titanium, the major hardening element, to concentrations fluctuating between 1 at.% at dendrite cores and up to 6% at dendrite interstices.

2. Chemical segregation in the weld results in the following modification of the aging response consistent with the resistance and hardness curves:

   a) Rapid initial precipitation in titanium enriched regions.

   b) Slower hardness response due to delayed aging of titanium depleted regions.

3. Slip localization occurs in the titanium depleted dendritic regions relative to the enriched interdendritic regions, resulting in an 'easy-path' of deformation.

4. Decreased weld microstructural coarseness or columnar grain size results in significant hardness increases.

5. Weldment hardness levels can be matched through post-weld solution annealing treatments prior to aging resulting in:

   a) Increased weld metal hardness.

   b) Decreased base metal hardness due to grain growth.

   c) Uniform deformation within the weld metal.

   d) More uniform strains across weld, HAZ and base metal regions.

6. The magnitude of the weldment strength mismatch decreases at cryogenic temperatures. This may be due to increased resistance to localized deformation by the inhibition of cross slip of widely split dislocations.

7. Weld metal segregation results in the formation of titanium-rich precipitates, believed to be the Chi (χ) topographically close-packed phase, not present in the base metal.

REFERENCES

1. D. Dew-Hughes: Cryogenics, Aug. 1975, p. 435.

2. D. Dew-Hughes: "Treatise on Materials Science and Technology," Vol. 14, Chapter 1, Academic Press, 1979.

3. R.E. Gold, W.A. Logsdon, G.E. Grotke, B. Lustman: "Advances in Cryogenic Engineering (Materials)," Vol. 28, Plenum Press, 1982.

4. C.D. Lundin, D.F. Spond: Welding Journal, Nov. 1976, p. 356s.

5. W.T. DeLong: Welding Journal, July 1974, p. 273s.

6. C.D. Lundin, W.T. DeLong, D.F. Spond: Welding Journal, Aug. 1975, p. 241s.

7. T.G. Gooch, Mrs. J. Honeycombe: Metal Construction & BWJ, March 1975, p. 146.

8. J.A. Brooks, R.W. Krenzer: Welding Journal, June 1974, p. 242s.

9. J.A. Brooks: Welding Journal, Nov. 1974, p. 517s.

10. J.G. Garland: Metal Construction & BWJ, April 1974, p. 121.

11. D.G. Telford, D.R. Milner: Metal Construction & BWJ, Dec. 1972, p. 461.

12. T. Edvardsson: "Solidification and Casting of Metals," p. 424, The Metals Society, 1979.

13. D.C. Brown et al: Welding Journal, June 1962, p. 241.

14. T.J. Headley, M.N. Karnousky, W.R. Sorenson: Met. Trans. A, March 1982, p. 345.

15. J.F. Henrietto, R.E. Lawther: J. Metals, Oct. 1978, p. 21.

16. V. Cihal, J. Kubelka: Practical Metall., Dec. 1975, p. 148.

17. D.G. Morris, D.R. Harries: Metal Science, Nov. 1978, p. 524.

18. G.V. Smith: Welding Journal, May 1956, p. 456.

19. L.K. Singhal, J.W. Martin: Acta Met., Vol. 16, 1968, p. 1441.

20. S.A. David, G.M. Goodwin, D.N. Braski: Welding Journal, Nov. 1979, p. 330s.

21. J.C. Lippold, W.F. Savage: Welding Journal, Dec. 1979, p. 362s.

22. C.E. Lyman: Welding Journal, July 1979, p. 189s.

23. W.T. DeLong: Welding Journal, July 1974, p. 273s.

24. G.A. Ratz, R.B. Gunia: Metals Progress, Jan. 1979, p. 76.

25. A.W. Brewer, R.L. Moment: Welding Journal, June 1976, p. 159s.

26. R.B. Gunia, G.A. Ratz: Welding Research Council (WRC) Bulletin 132, Aug. 1968.

27. C. Syn, H.K. Shin, M.J. Strum: unpublished research, LBL, 1980.

28. F.G. Wilson, F.B. Pickering: Acta Met., Jan. 1968, Vol. 16, p. 115.

29. H. Herman, J.B. Cohen, M.E. Fine: Acta Met., 1963, Vol. 11, p. 43.

30. N.F. Mott: J. Inst. Metals, 1937, Vol. 60, p. 267.

31. R.F. Decker: "Source Book on Materials for Elevated Temperature Applications," E.F. Bradley ed., p. 275, American Society for Metals, 1979.

32. H.J. Beattie, Jr., W.C. Hagel: J. Metals, July 1957, p. 911.

33. K.M. Chang: Ph.D. Thesis, LBL-9208, May 1979.

34. W.F. Savage, B.M. Krantz: Welding Journal, July 1971, p. 292s.

35. H. Homma, M. Mori, K. Shinmyo: Welding Journal, Sept. 1979, p. 277s.

36. P.P. Puzak, W.R. Apblett, W.S. Pellini: Welding Journal, Jan. 1956, p. 9s.

37. J.C. Borland, R.N. Younger: Metal Construction & BWJ, Jan. 1960, p. 22.

38. P. Sullivan, M.J. Donachie, Jr.: "Source Book on Materials for Elevated Temperature Applications," E.F. Bradley ed., p. 239, American Society for Metals, 1979.

39. H.J. Beattie Jr., W.C. Hagel: Trans. of Metall. Soc. of AIME, Feb. 1961, Vol. 221, p. 28.

40. B.R. Clark. F.B. Pickering: J. Iron & Stl. Inst., Jan. 1967, Vol. 205, p. 70.

41. W.A. Owzcarski, C.P. Sullivan: Welding Journal, June 1965, p. 241s.

42. R. Blower, S. Mayer: J. Iron & Stl. Inst., Nov. 1963, Vol. 201, p. 933.

TABLE 1

LARGE COIL PROJECT (LCP) CONDUCTOR JACKET

MATERIAL PERFORMANCE REQUIREMENTS

PROPERTY	DESIGN REQUIREMENT	PROPOSED ACCEPTANCE CRITERIA
TENSILE YIELD STRENGTH AT 4 K MPa (Ksi)	1014 (147)	>1034 (>150)
FRACTURE TOUGHNESS AT 4K MPa $\sqrt{m}$ (Ksi$\sqrt{in}$)	27.5 (25) (0.25 mm crack)	>55 (>50)
TENSILE ELONGATION AT 4K (%)	--	>5

TABLE 2

NITRONIC 40 CHEMICAL ANALYSES

	Fe	Cr	Ni	Mn	C	N	Si	S	P
Sheet Material	--	20.2	7.15	9.03	.016	0.34	--	--	--
Plate Material	--	20.3	7.06	9.04	.019	0.36	--	--	--
Armco Specifications	bal	19.0 21.5	5.50 7.50	8.00 10.0	.040 max	0.15 0.40	1.00 max	.030 max	.060 max

TABLE 3

JBK-75 CHEMICAL ANALYSES

	Fe	Cr	Ni	Ti	Al	Mo	V	Mn	Si	C	P	S	B
Heat 1	bal	15.5	29.8	2.05	0.24	1.25	0.27	0.05	.018	.016	.002	18PPM	<5PPM
Heat 2	bal	14.4	28.5	2.15	0.20	1.20	0.27	--	--	.016	.005	.006	.0018
A-286	bal	14.5	25.4	2.25	0.22	1.30	0.26	1.50	0.58	.063	.004	.005	.0073

TABLE 4

JBK-75 WELDING CONDITIONS

Autogenous GTA Butt Welds

Sheet Thickness	Voltage	Amperage	Travel Speed (mm/min)	Heat Input	Gases (Argon) Shield	Backing
1.5 mm	10v.	65 A.	250	0.15 kJ/mm	15 cfh	15 cfh
3.2 mm	12v.	170 A.	250	0.48 kJ/mm	15 cfh	15 cfh

TABLE 5

NITRONIC 40 TENSILE PROPERTIES

Flat Tensile Specimen (25.4 mm Gage)

Condition	Test Temperature	Y.S. (MPa)	T.S. (MPa)	Elongation (%)
Cold Worked 10%	298 K	690	910	20
	77 K	1475	1740	14
Cold Worked 10% + Aged 700°C, 30 hrs.	298 K	710	910	27
	77 K	1360	1660	18
	4 K	1460	1915	16
G.T.A. Welded	298 K	469	738	21
	77 K	1080	1470	13
G.T.A. Welded + Aged 700°C, 30 hrs.	298 K	483	793	25
	77 K	1150	1310	1.1 (1.5,0.7)

TABLE 6

NITRONIC 40 MAGNETIC PERMEABILITY MEASUREMENTS

Condition	Region	Magnetic Permeability Indication*
As Welded	Base	<1.01
	Weld	1.05
Welded + Aged	Base	<1.01
	Weld	<1.01

* Severn Engr. Co. permeability indicator

TABLE 7

NITRONIC 40 CHARPY IMPACT ENERGY DATA

Condition	Test Temperature	C_v , Joules (ft-lbs)
As Annealed	298 K	137 (101)
	77 K	69 (51)
Annealed Cold Worked 10% Aged 30 hrs. 700°C	298 K	114 (84)
	77 K	8.8 (6.5)

TABLE 8

G.T.A. WELDED JBK-75 TENSILE DATA

Standard Heat Treatment ; 700°C for 30 hrs.

Conditions	Yield Strength MPa (Ksi)	Tensile Strength MPa (Ksi)	Elongation (25.4 mm Gage)
298 K	772 (112)	924 (134)	4.5 %
77 K	814 (118)	1240 (180)	13.5 %
4 K	979 (142)	--	10.0 %

TABLE 9

JBK-75 TENSILE DATA AT 77K

Conditions	Yield Strength MPa (Ksi)	Tensile Strength MPa (Ksi)	Elongations 25.4 mm	12.7 mm	6.3 mm
Aged 725°C 40 hrs. + 650°C 24 hrs.					
Base Metal	1115 (162)	1530 (222)	21 %	21 %	
G.T.A.W. Specimen	1000 (145)	1300 (188)	6.5 %	10 %	18 %
Aged 725°C 50 hrs. + 650°C 24 hrs.					
Base Metal	1105 (160)	1525 (221)	21 %	21 %	
G.T.A.W. Specimen	979 (142)	1255 (182)	5.8 %	8.1 %	15 %
Cold Worked 10 % Aged 725°C 40 hrs. + 650°C 24 hrs.					
Base Metal	1220 (177)	1615 (234)	20 %	21 %	
G.T.A.W. Specimen	1160 (168)	1385 (201)	3.8 %	6.5 %	12 %

TABLE 10

JBK-75 TEMPERATURE DEPENDENCE OF TENSILE PROPERTIES

Standard Heat Treatment; 24 hrs. 725°C + 24 hrs. 650°C

Conditions		Yield Strength MPa (Ksi)	Tensile Strength MPa (Ksi)	Elongations 25.4 mm	12.7 mm	6.3 mm	Reduction in Area (%)
298 K	Base	965 (140)	1215 (176)	17	21		41
	Weld	841 (122)	945 (137)	4	7.5	16	26
77 K	Base	1105 (160)	1530 (222)	23	25		27
	Weld	972 (141)	1215 (176)	6	10	19	32
4.2 K	Base	1180 (171)	1600 (232)	16	14		33
	Weld	1130 (164)	1385 (201)	6.5	11	21	32

FIGURE CAPTIONS

Figure 1 Circuit diagram for resistance measurements.

Figure 2 Experimental set-up for resistance measurements.

Figure 3 Nitronic 40 weld microstructure before and after aging 30 hours at 700°C, electrolytic etch in oxalic acid.

Figure 4 Nitronic 40 tensile fracture mode vs. weld microstructure before and after aging 30 hours at 700°C, mixed acid etch.

Figure 5 Nitronic 40 Charpy impact specimen fractographs.

Figure 6 Temperature dependence of JBK-75 yield and tensile strength.

Figure 7 Resistance changes during isothermal aging of JBK-75 at 725°C.

Figure 8 Hardness curves of JBK-75 aged at 725°C.

Figure 9 Hardness curves of JBK-75 aged at 700°C.

Figure 10 Hardness curves of JBK-75 given 25% post weld cold work before aging at 725°C.

Figure 11 Cellular precipitate in JBK-75 weld metal aged 260 hours at 725°C, electrolytic etch in oxalic acid.

Figure 12 JBK-75 weld metal solidification structure.

Figure 13 JBK-75 weld metal solidification structure.

Figure 14 Titanium concentration profile in as-welded JBK-75 weld metal.

Figure 15 Slip localization in as-polished and deformed JBK-75 weldment aged 24 hrs. 725°C.

Figure 16 Slip localization in as-polished and deformed JBK-75 weldment annealed 10 hrs. @ 950°C before aging 24 hrs. 725°C.

Figure 17 Hardness curves of annealed JBK-75 weldments aged 24 hrs. 725°C.

Figure 18 Hardness curves of as-annealed JBK-75 weldments.

Figure 19 Coring in as-welded vs. annealed JBK-75 welds aged 24 hrs. 725°C, mixed acid etch.

Figure 20 Slip localization in as-polished and deformed JBK-75 recrystallized weld metal.

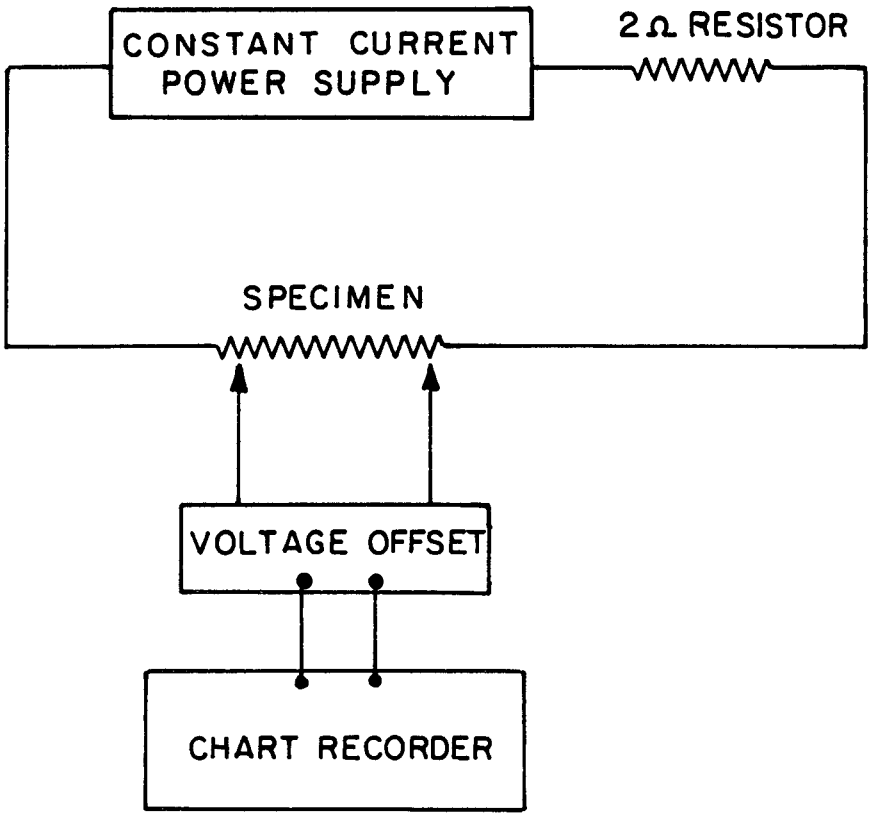

XBL823-5387

Fig. 1

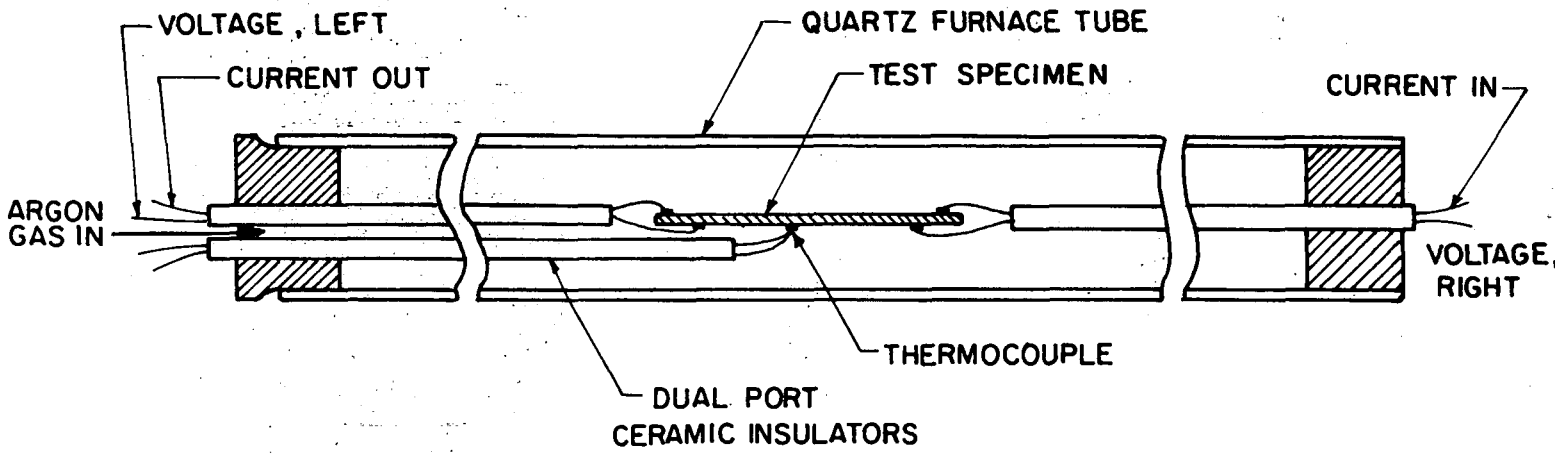
VOLTAGE, LEFT
CURRENT OUT
QUARTZ FURNACE TUBE
TEST SPECIMEN
CURRENT IN
ARGON
GAS IN
VOLTAGE,
RIGHT
THERMOCOUPLE
DUAL PORT
CERAMIC INSULATORS
XBL 823-5386

Fig. 2

10μ

N40 As Welded

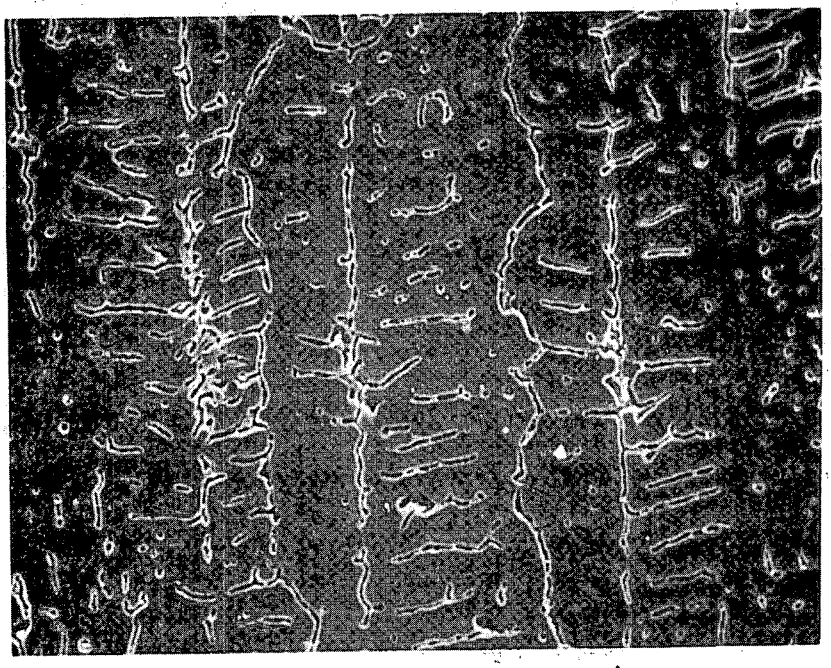

N40 Welded & Aged

XBB 823-2612

Fig. 3

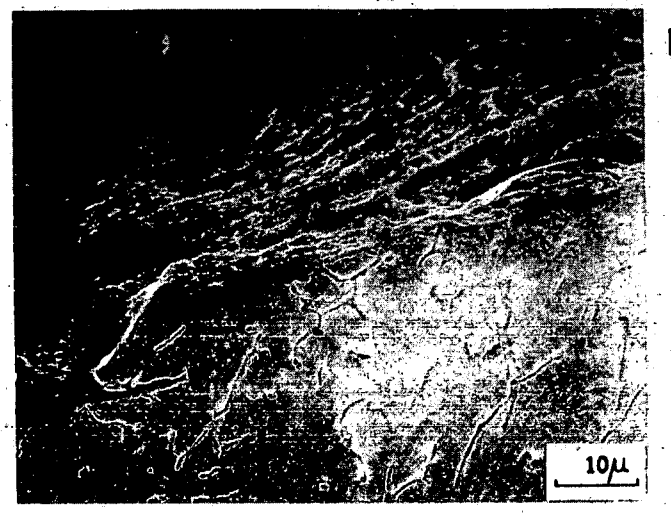

FRACTURE MODE VS WELD MICROSTRUCTURE
NITRONIC 40 TENSILE SPECIMEN

LEFT: AS WELDED, LNT

BELOW: WELDED & AGED, LNT

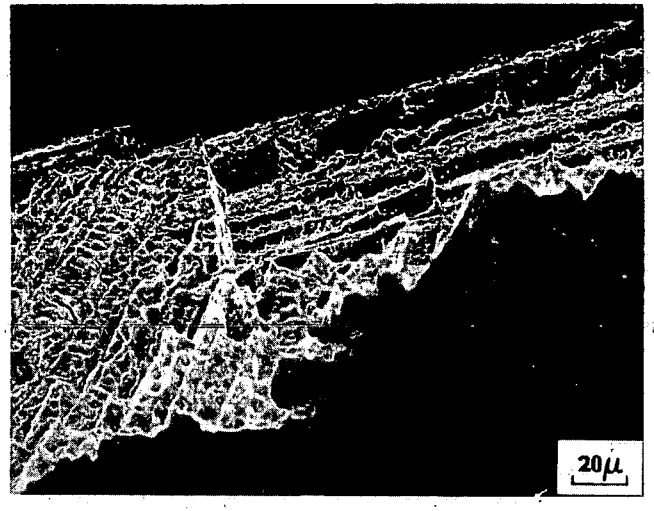

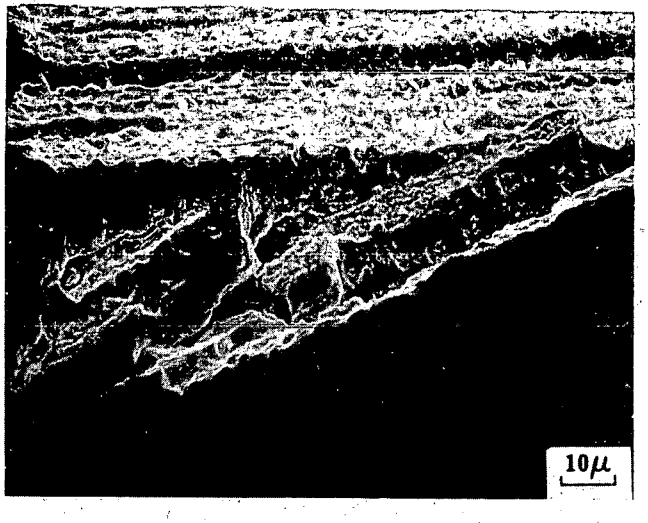

XBB 822-1442

Fig. 4

NITRONIC 40 CHARPY IMPACT SPECIMEN FRACTOGRAPHS

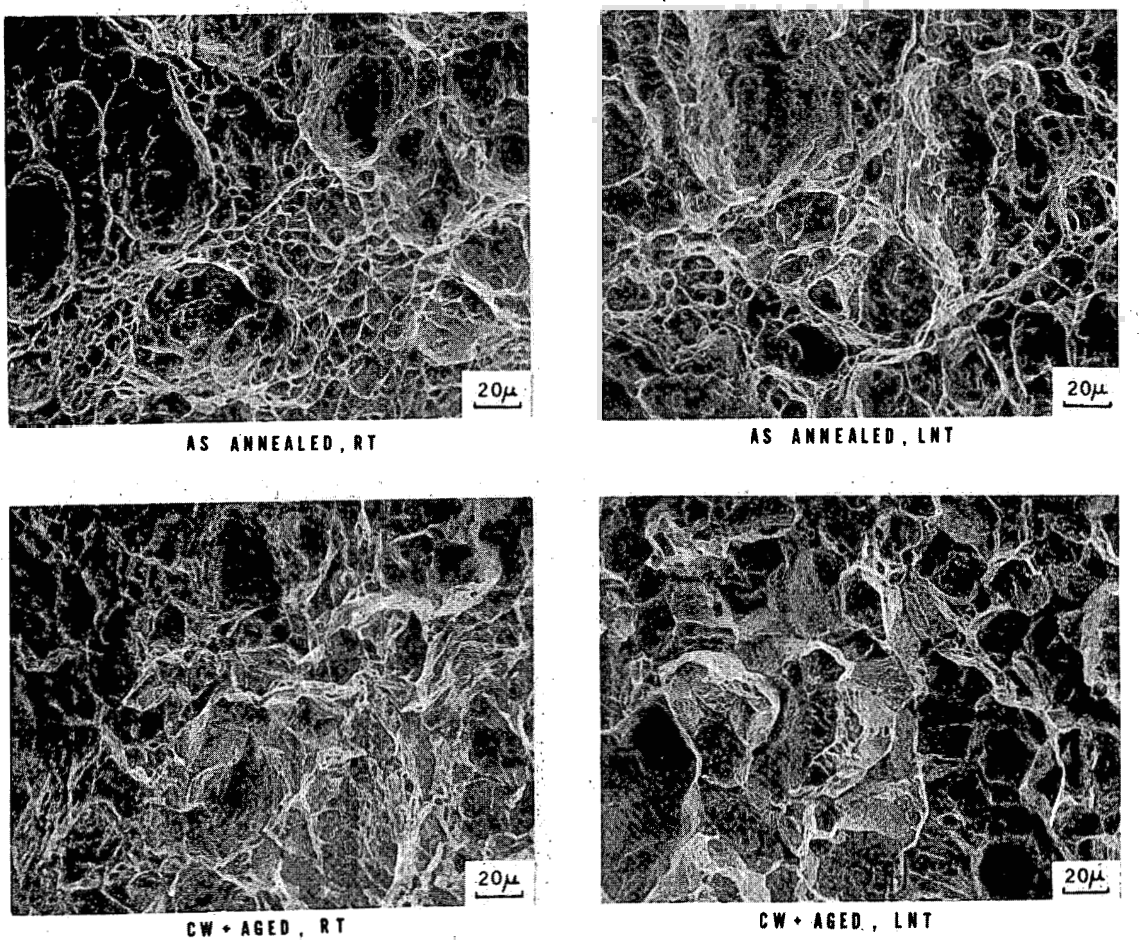

XBB 822-1440

Fig. 5

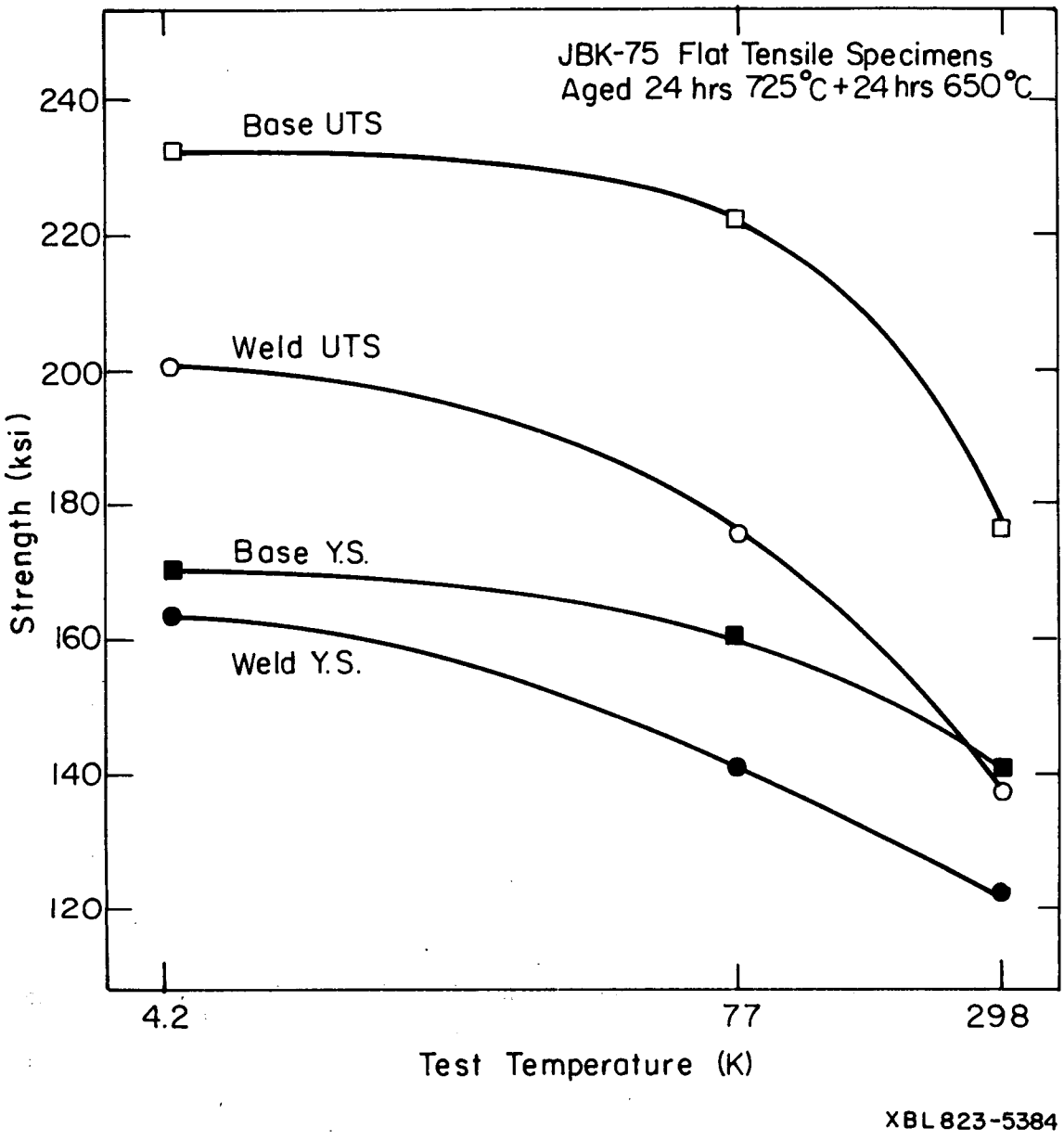
JBK-75 Flat Tensile Specimens
Aged 24 hrs 725°C + 24 hrs 650°C
Base UTS
Weld UTS
Base Y.S.
Weld Y.S.
240
220
200
180
160
140
120
Strength (ksi)
4.2
77
298
Test Temperature (K)
XBL823-5384

Fig. 6

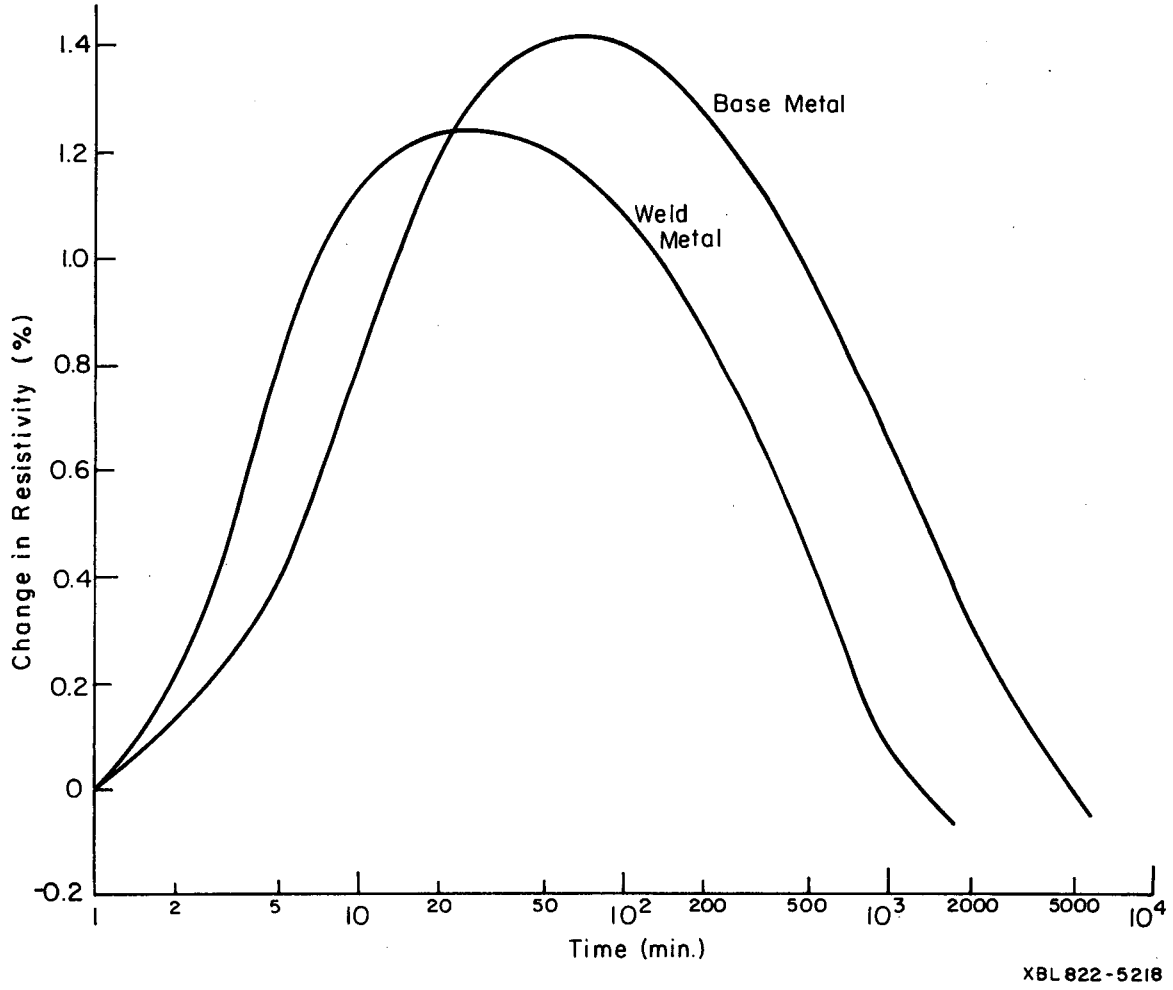
1.4
1.2
1.0
0.8
0.6
0.4
0.2
0
-0.2
Change in Resistivity (%)
Base Metal
Weld
Metal
1
2
5
10
20
50
10^2
200
500
10^3
2000
5000
10^4
Time (min.)
XBL822-5218

Fig. 7

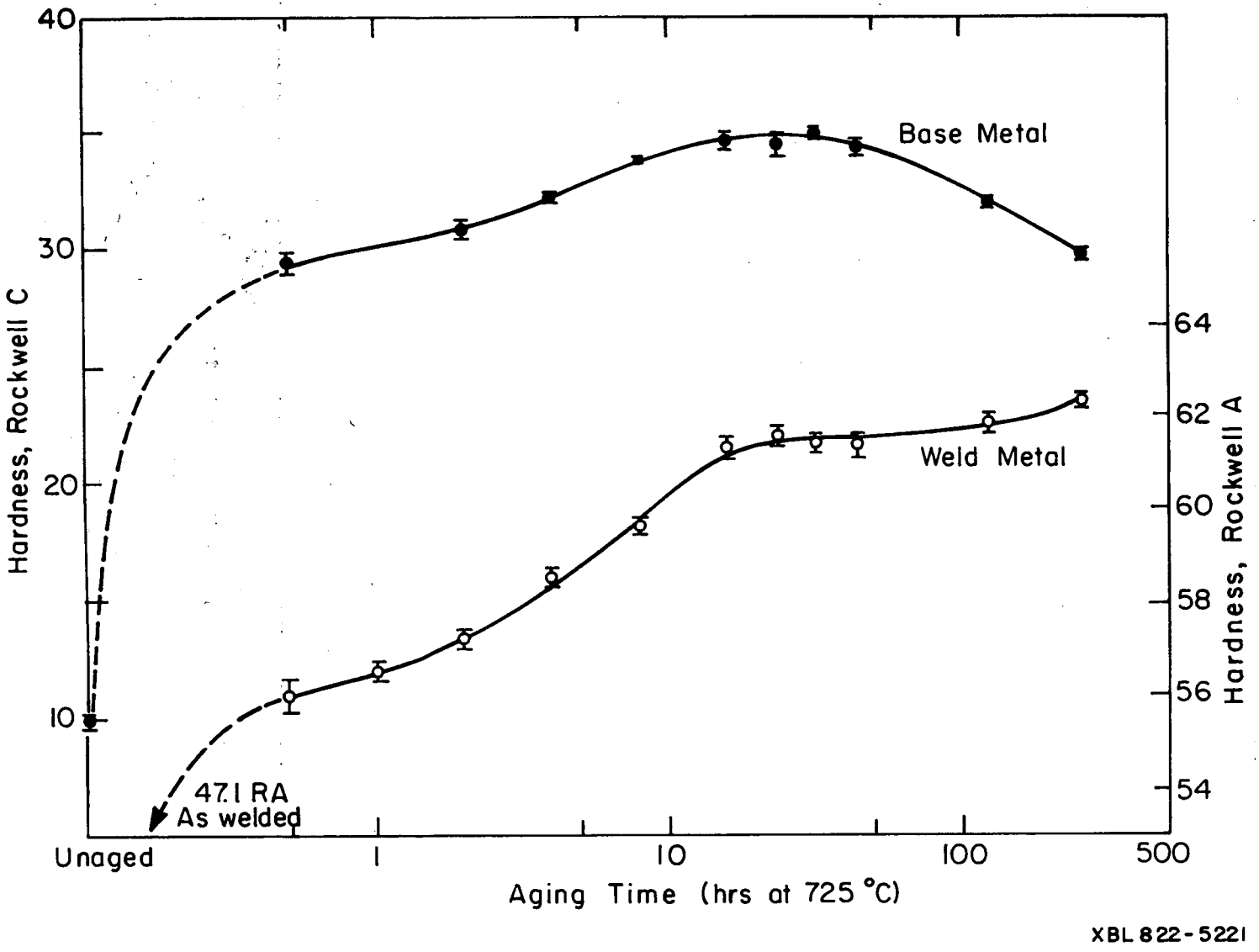
40
30
20
10
Hardness, Rockwell C
64
62
60
58
56
54
Hardness, Rockwell A
Base Metal
Weld Metal
47.1 RA
As welded
Unaged
1
10
100
500
Aging Time (hrs at 725 °C)
XBL 822-5221

Fig. 8

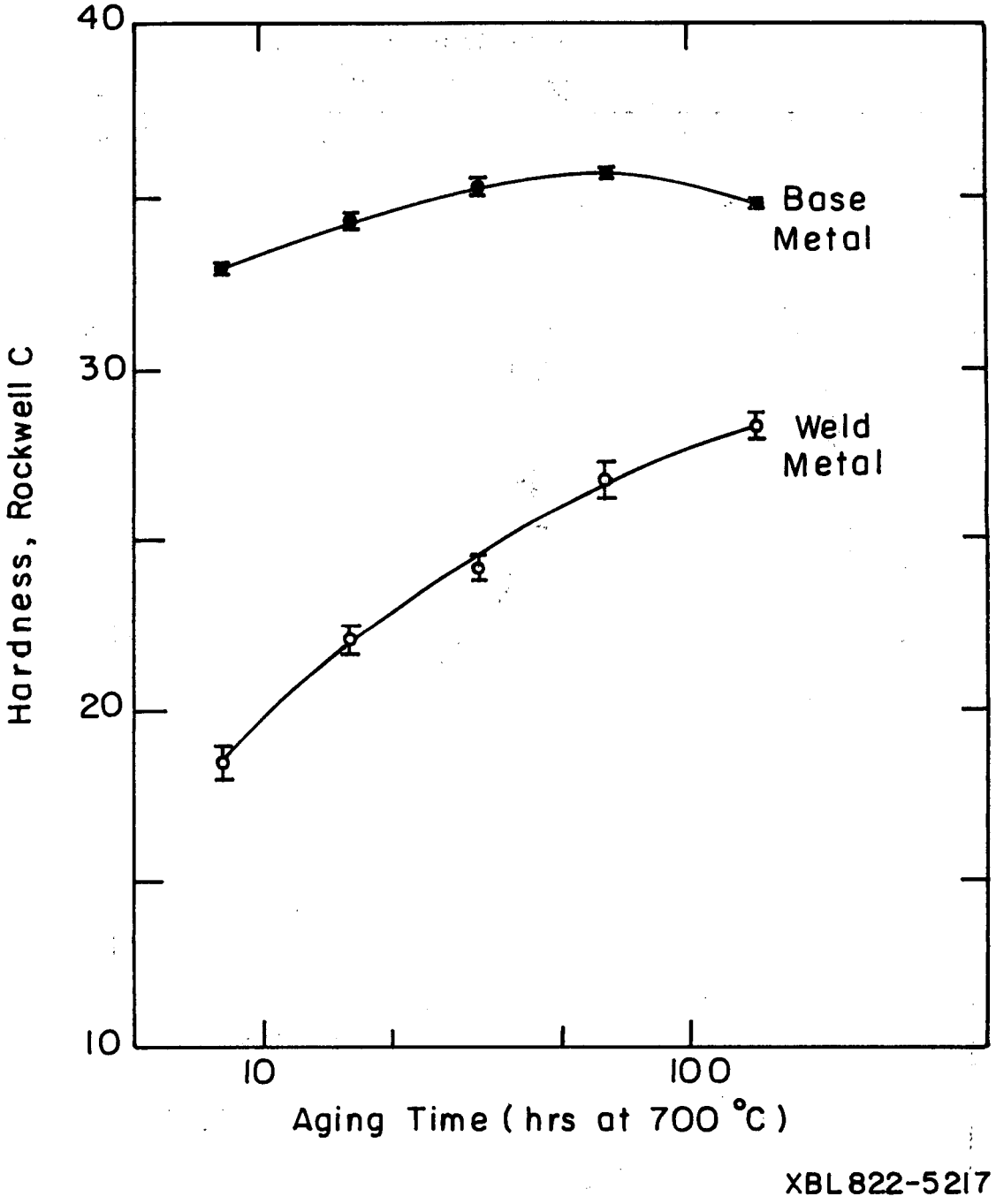
40
30
20
10
Hardness, Rockwell C
Base
Metal
Weld
Metal
10
100
Aging Time (hrs at 700 °C)
XBL822-5217

Fig. 9

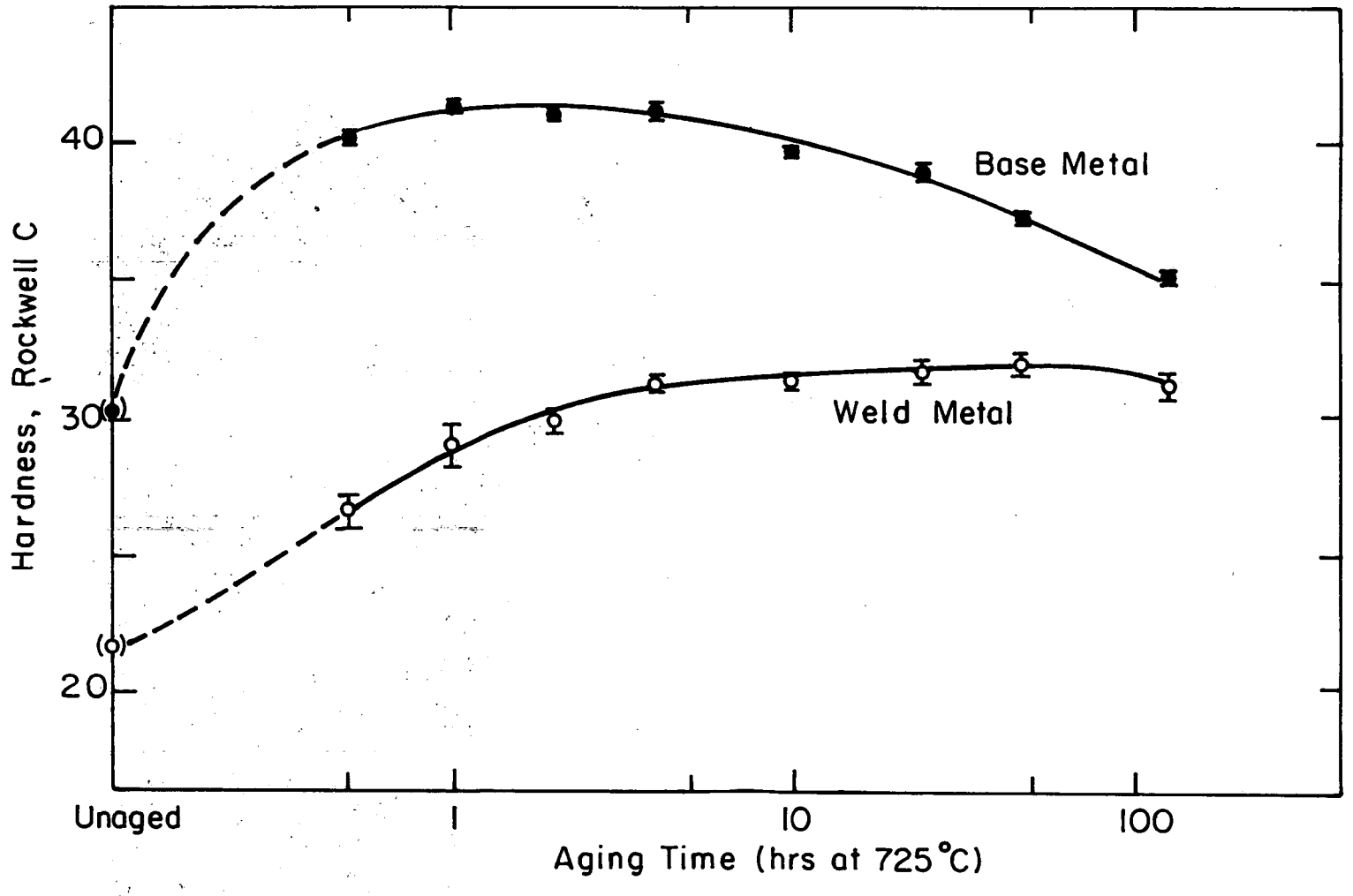
Hardness, Rockwell C
40
30
20
Base Metal
Weld Metal
Unaged
1
10
100
Aging Time (hrs at 725°C)
XBL 822-5220

Fig. 10

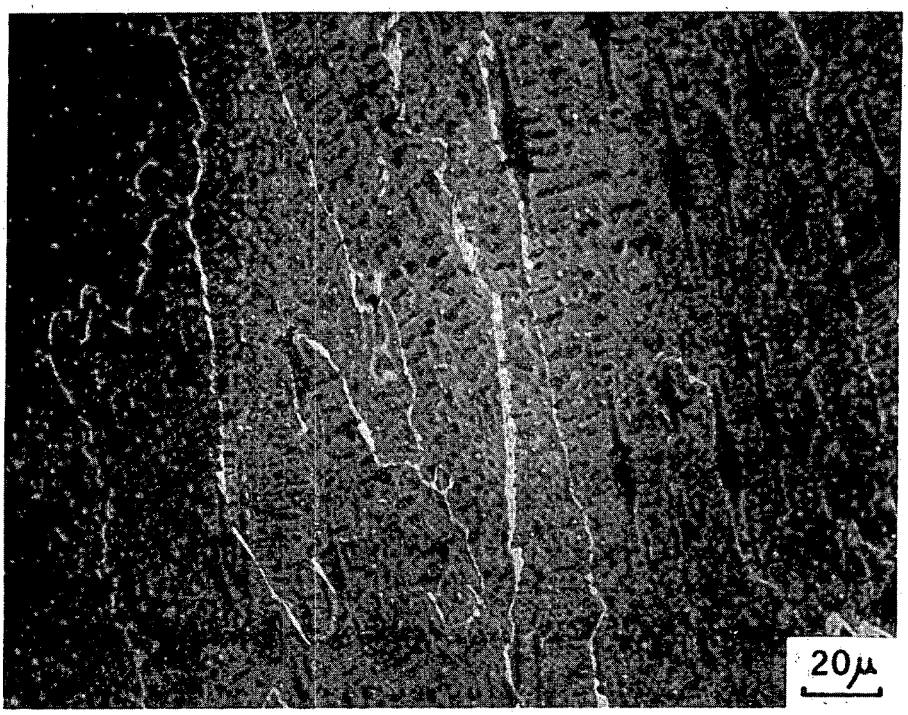

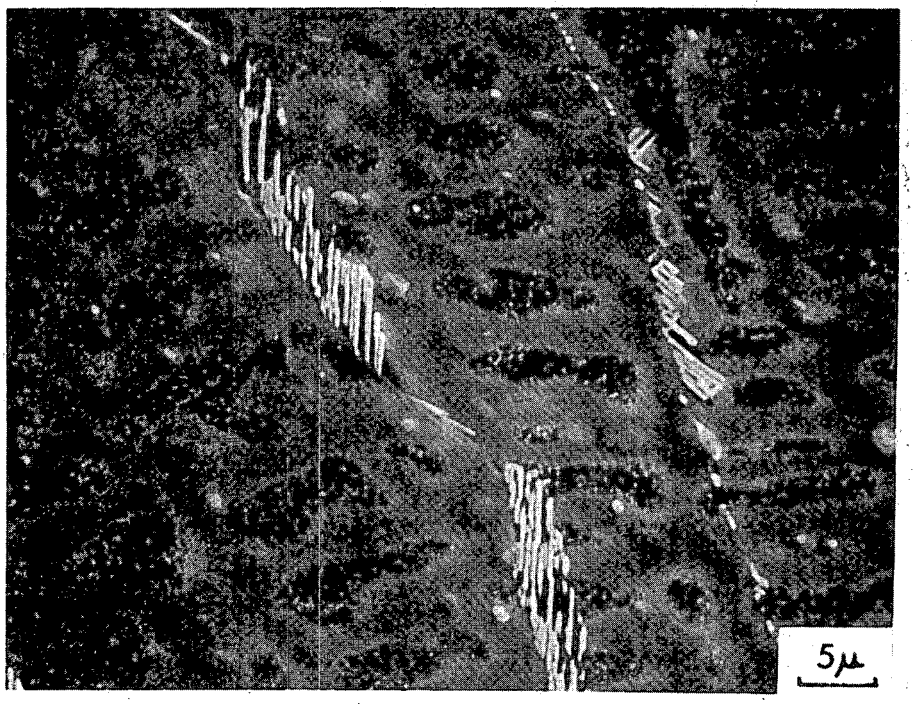

XBB 823-2785

Fig. 11

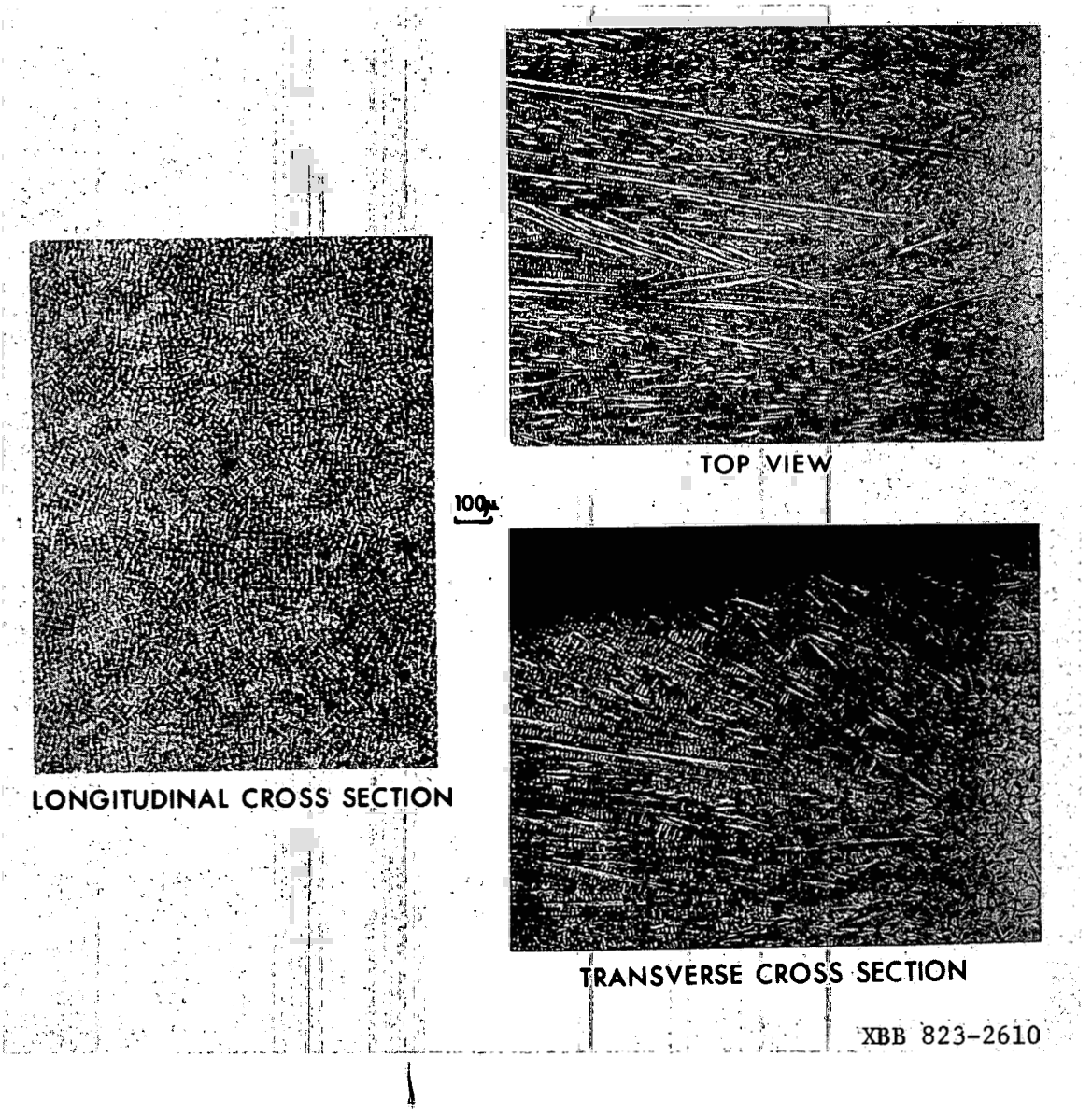
TOP VIEW
100μ
LONGITUDINAL CROSS SECTION
TRANSVERSE CROSS SECTION
XBB 823-2610

Fig. 12

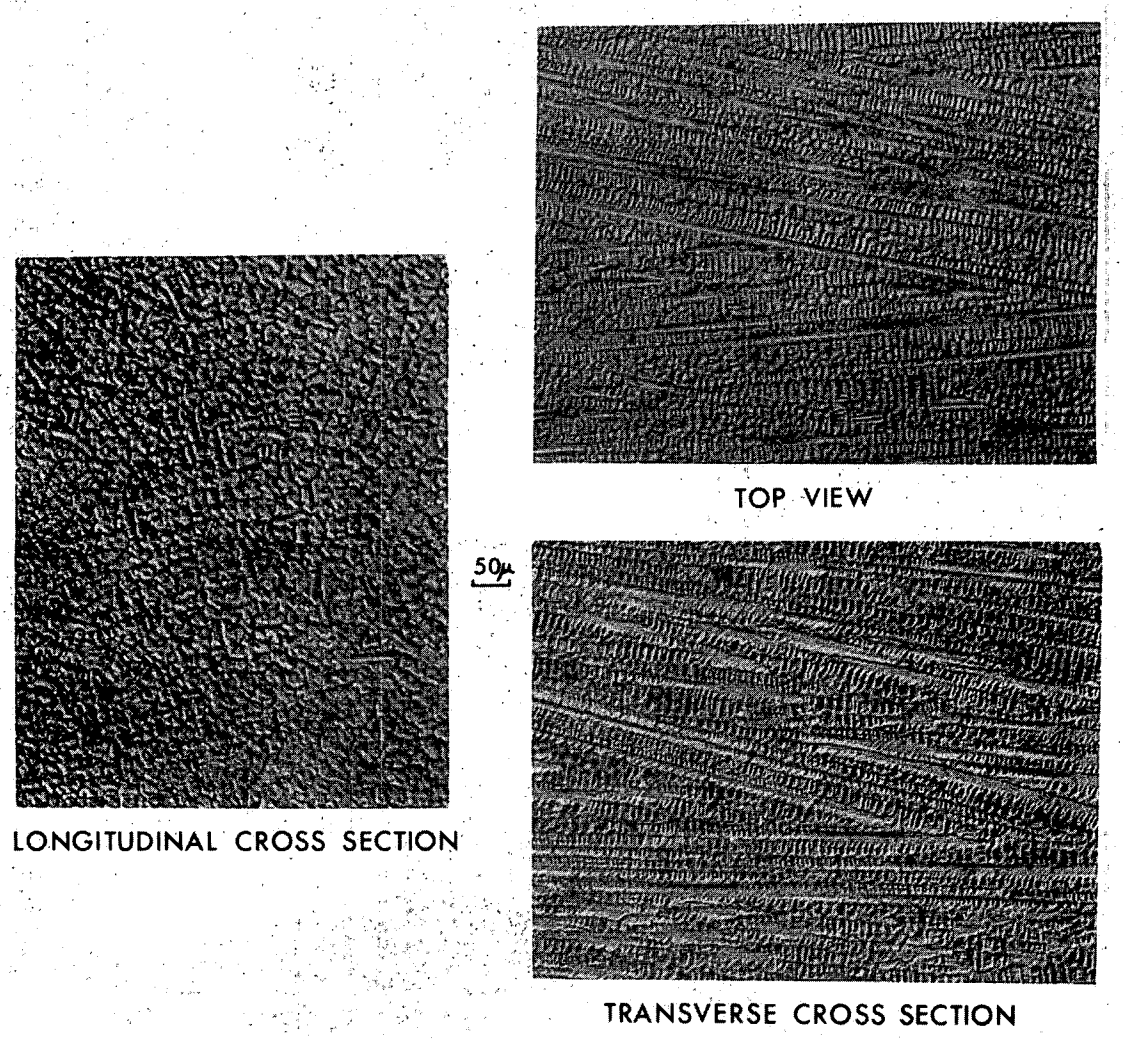

XBB 823-2611

Fig.13

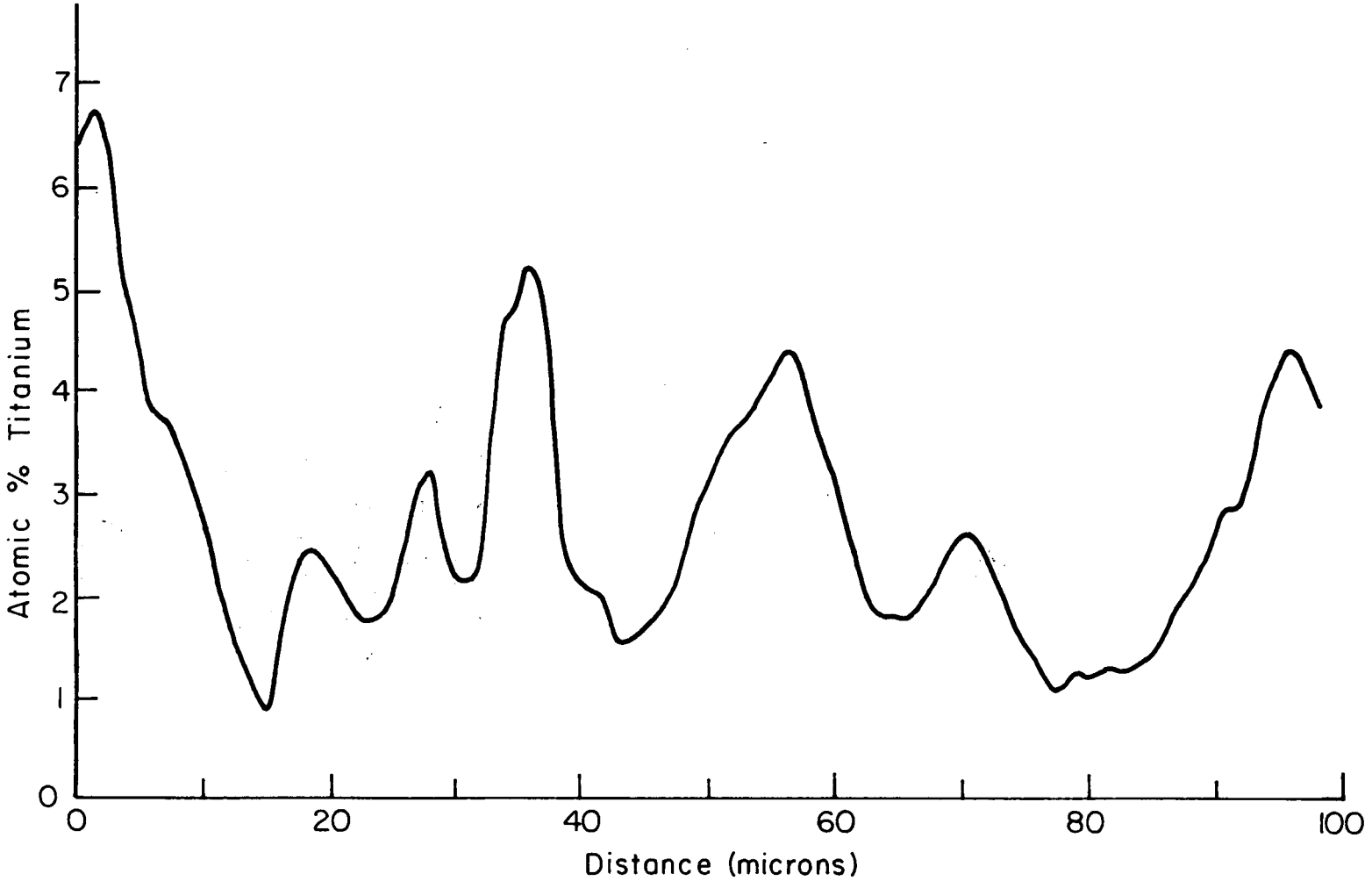

XBL 822-8073

Fig. 14

XBB 822-1438

Fig. 15

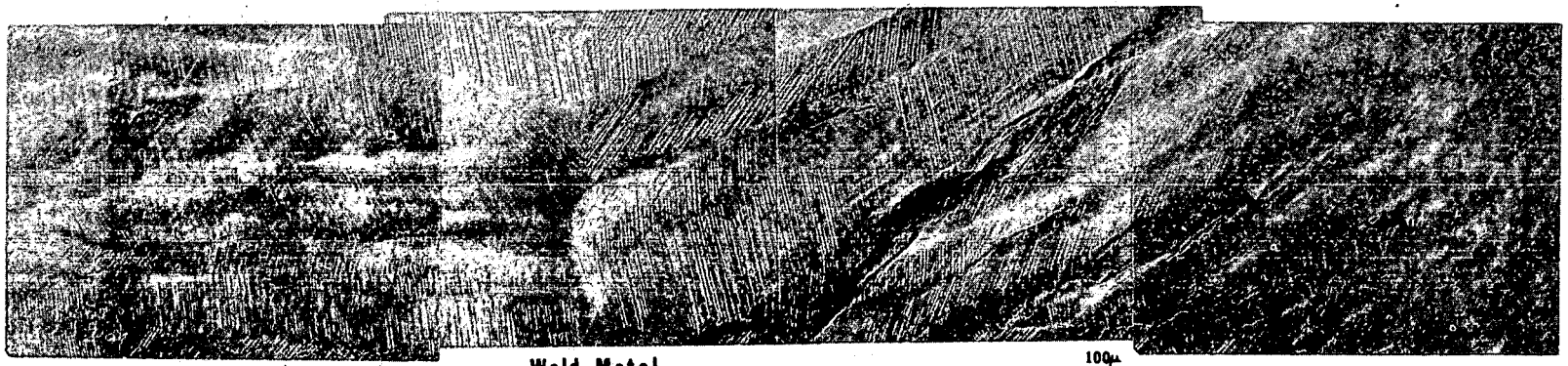

XBB 822-1441

Fig. 16

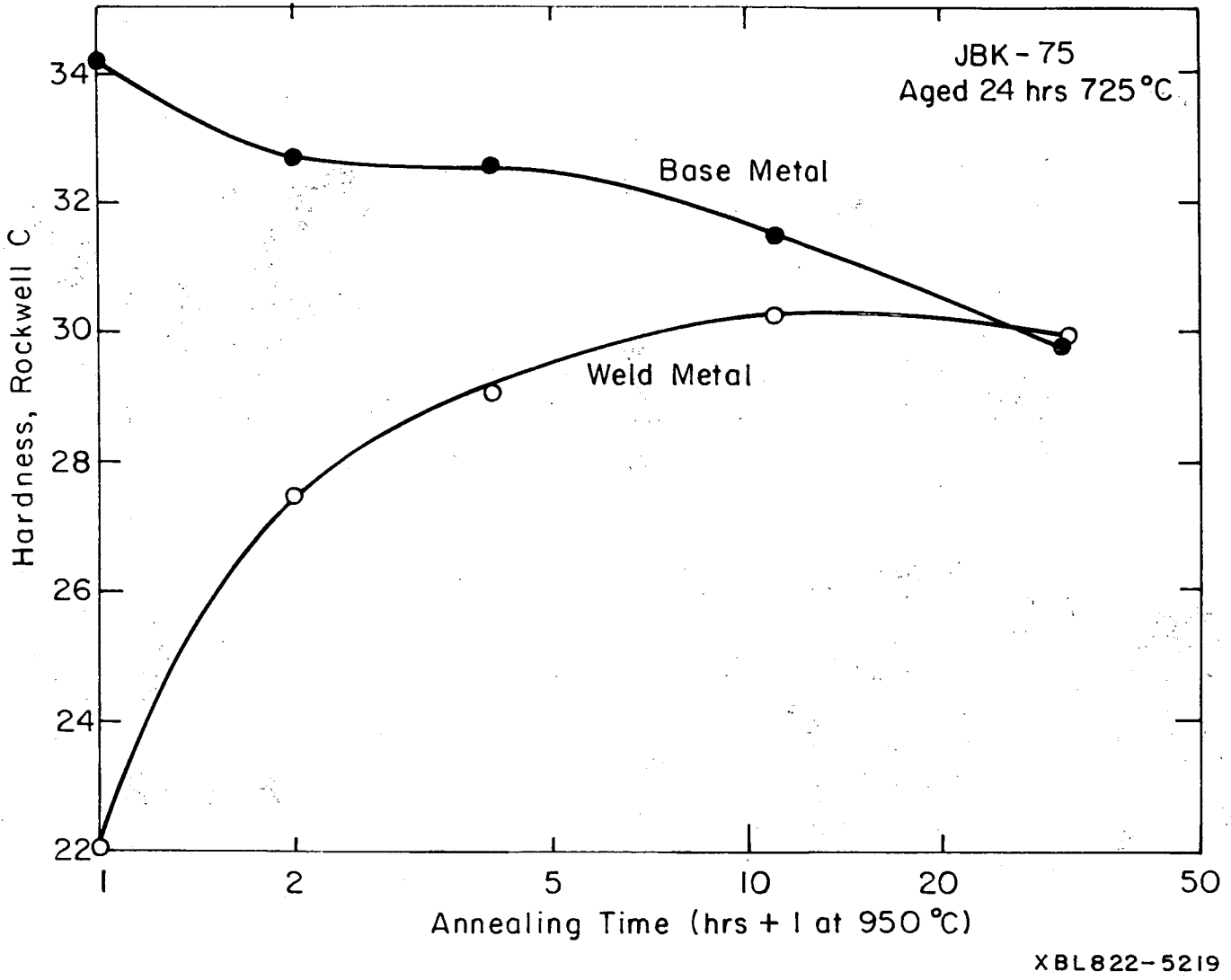
JBK - 75
Aged 24 hrs 725°C
Base Metal
Weld Metal
Hardness, Rockwell C
34
32
30
28
26
24
22
1
2
5
10
20
50
Annealing Time (hrs + 1 at 950°C)
XBL822-5219

Fig. 17

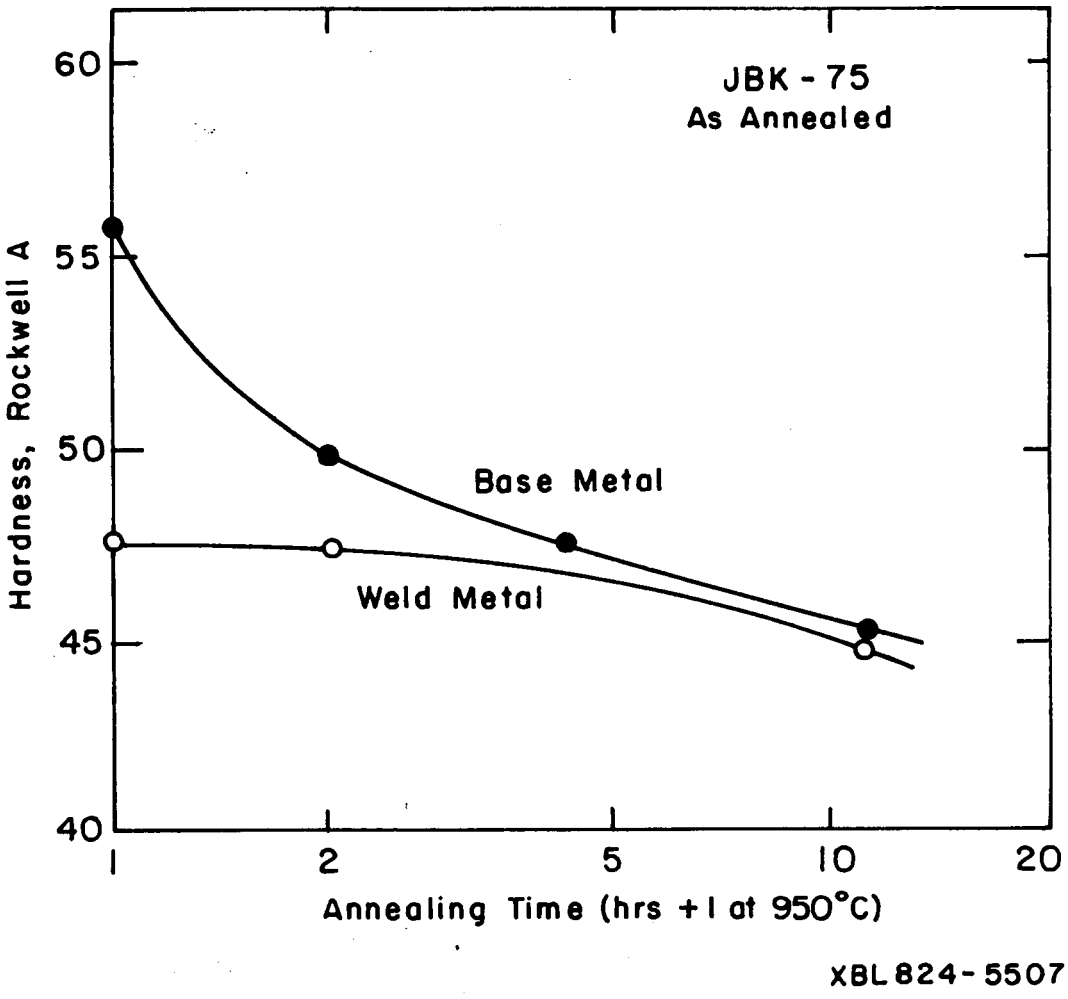
JBK - 75
As Annealed
Base Metal
Weld Metal
Hardness, Rockwell A
60
55
50
45
40
1
2
5
10
20
Annealing Time (hrs + 1 at 950°C)
XBL 824-5507

Fig. 18

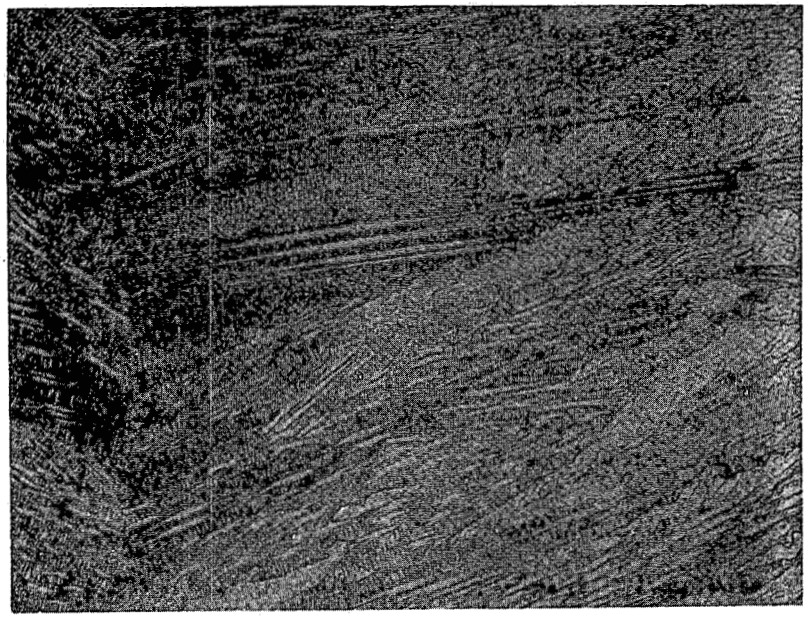

As Welded & Aged

100μ

Annealed 30 hrs @ 950°C

XBB 823-2613

Fig. 19

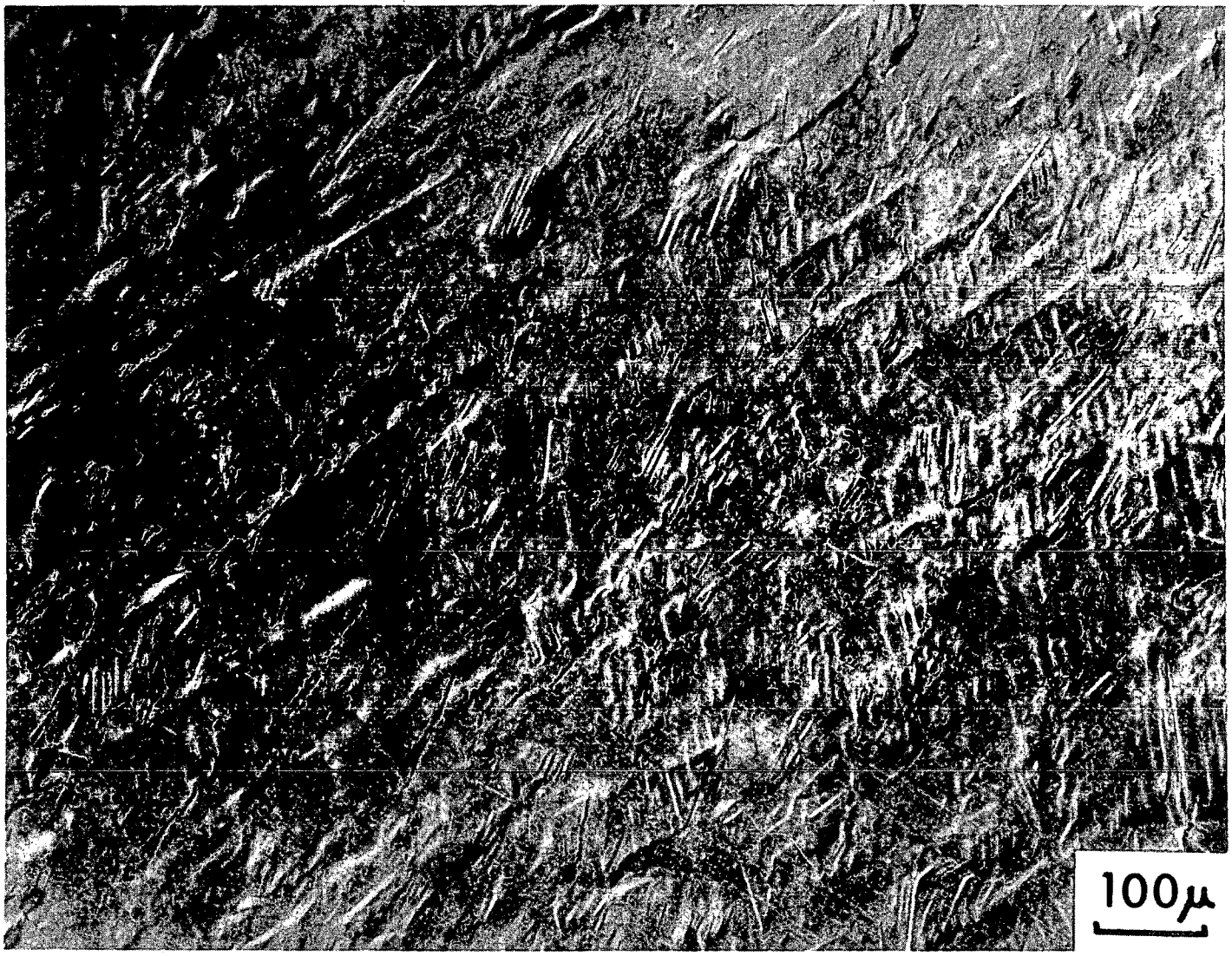

XBB 823-2784

Fig. 20

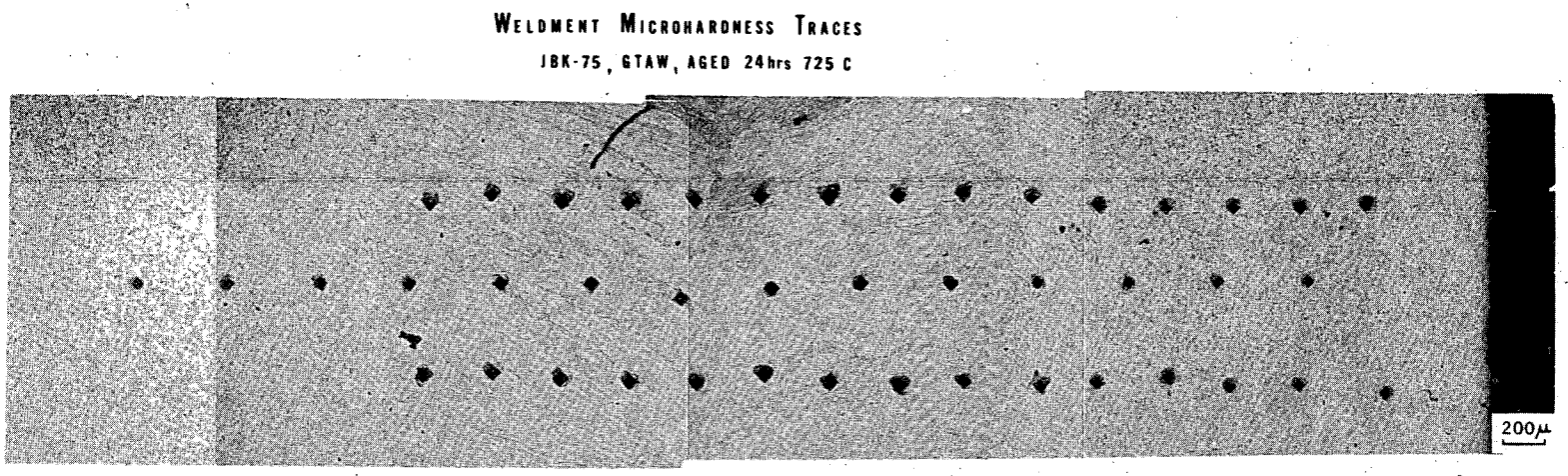

XBB 822-1439

Fig. 21

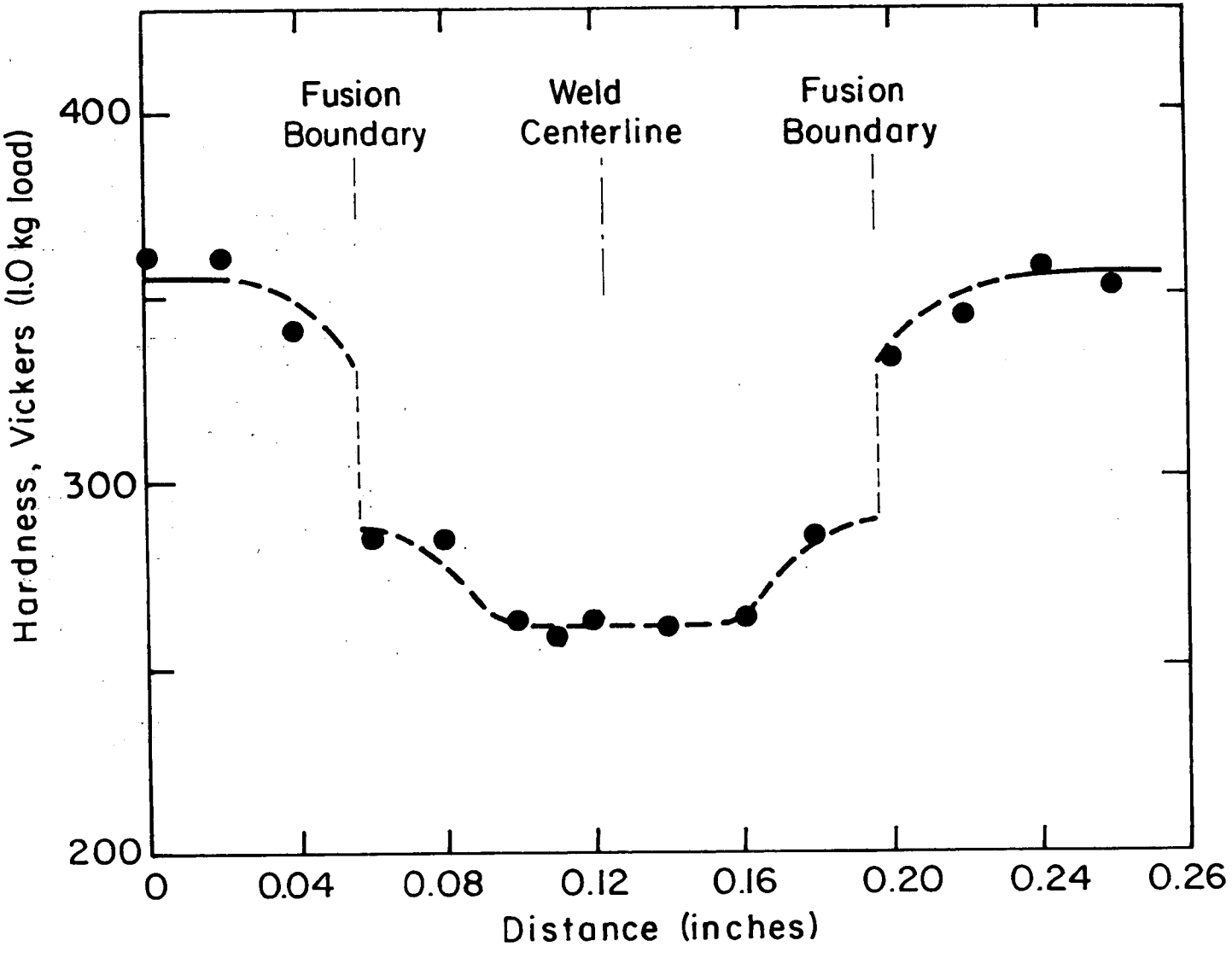

Fig. 22

XBL822-5222

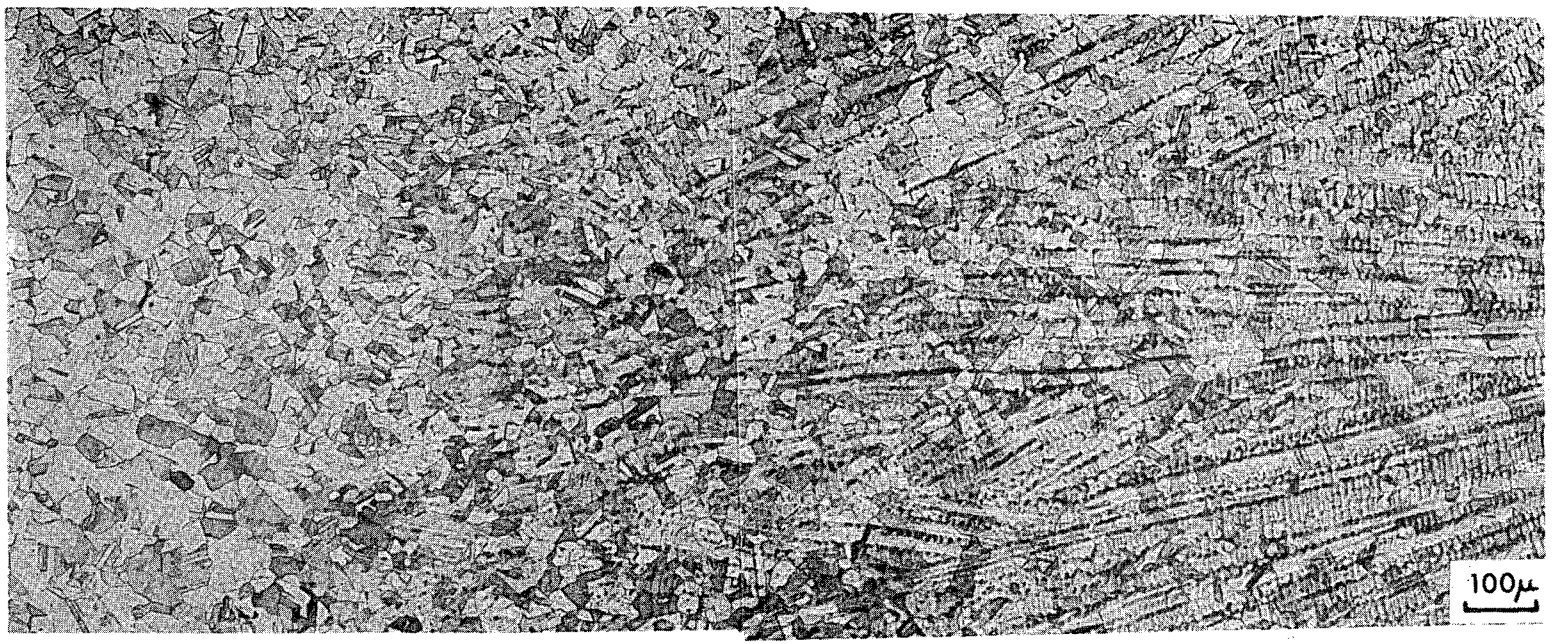

XBB 822-1437

Fig. 23

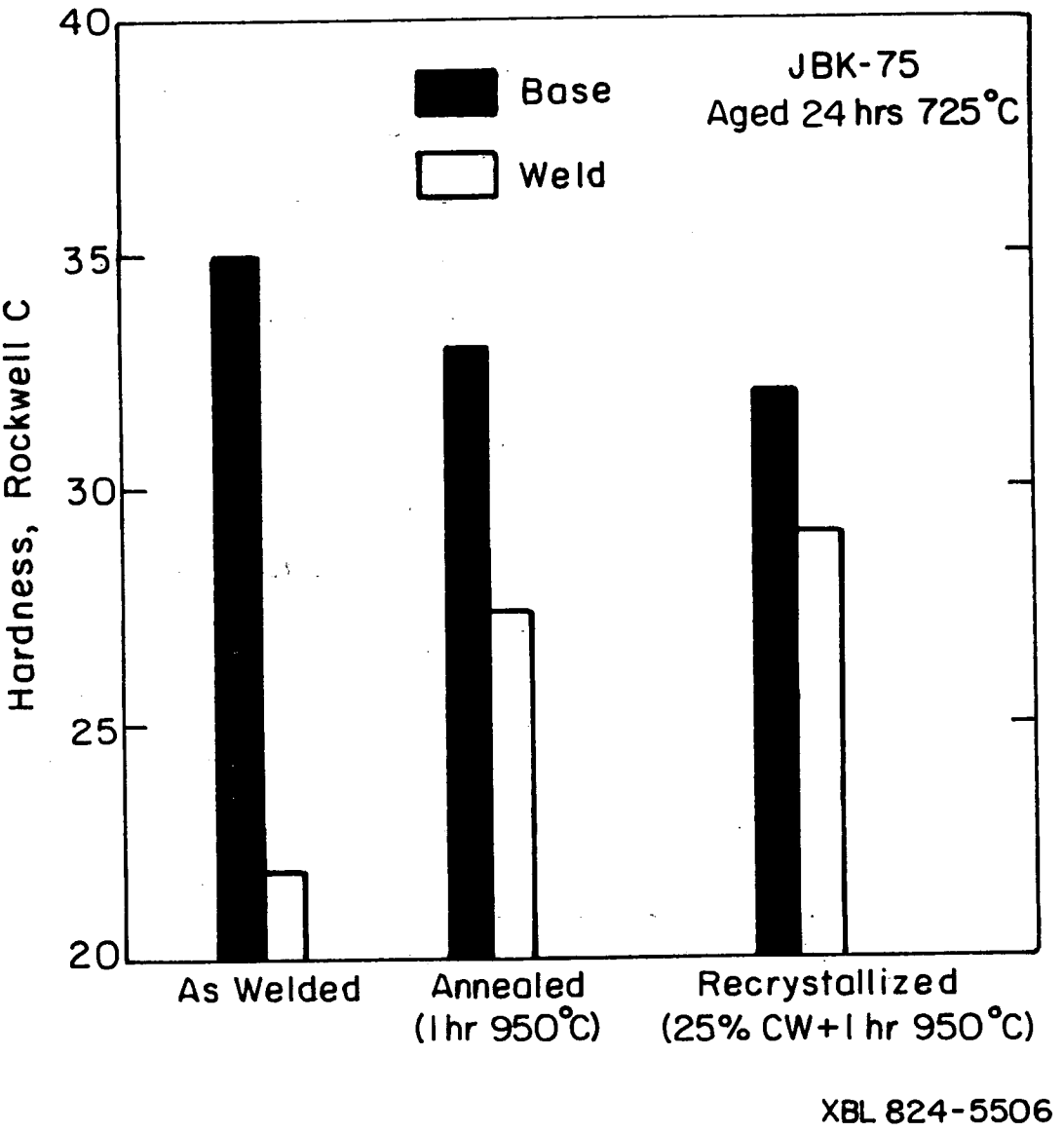
40
35
30
25
20
Hardness, Rockwell C
Base
Weld
JBK-75
Aged 24 hrs 725°C
As Welded
Annealed
(1 hr 950°C)
Recrystallized
(25% CW+1 hr 950°C)
XBL 824-5506

Fig. 24

ACKNOWLEDGEMENTS

I would like to express my gratitude to all involved in the successful completion of this work. Special thanks are extended to my research advisor, J.W. Morris Jr. , for his support and to all of the helpful and inspirational members of the research group, as well as the expert technical staff at the Materials and Molecular Research Division, Lawrence Berkeley Laboratory. I am also very fortunate to have received the enduring love and patient support of my wife, Wendy, and my entire family.

The materials used in this investigation were kindly provided by E.N.C. Dalder, Lawrence Livermore Laboratory and T.J. Headley, Sandia Albuquerque.

This work was supported by the Director, Office of Energy Research, Office of Development and Technology, Magnetic Systems Division and the Office of Basic Energy Sciences, Materials Sciences Division of the U.S. Department of Energy under Contract Number DE-AC03-76SF00098.